Deposition, Characterization and Process Optimization of Molybdenum Thin Films using DC-Plasma Magnetron Sputtering for Back Contact Application in CIGS based Thin Films Solar Cells

A Thesis submitted to Department of Materials Engineering, School of Chemical and Materials Engineering (SCME), NUST, in partial fulfillment of the requirements for the degree of

MASTER OF SCIENCE (MS)
In
MATERIALS AND SURFACE ENGINEERING

By
MAJID KHAN
2009-NUST-MS Ph.D-MS-E-03

Supervised By
DR. MOHAMMAD ISLAM

SCHOOL OF CHEMICAL AND MATERIALS ENGINEERING (SCME),
NATIONAL UNIVERSITY OF SCIENCES AND TECHNOLOGY (NUST),
H-12, ISLAMABAD, PAKISTAN
2011

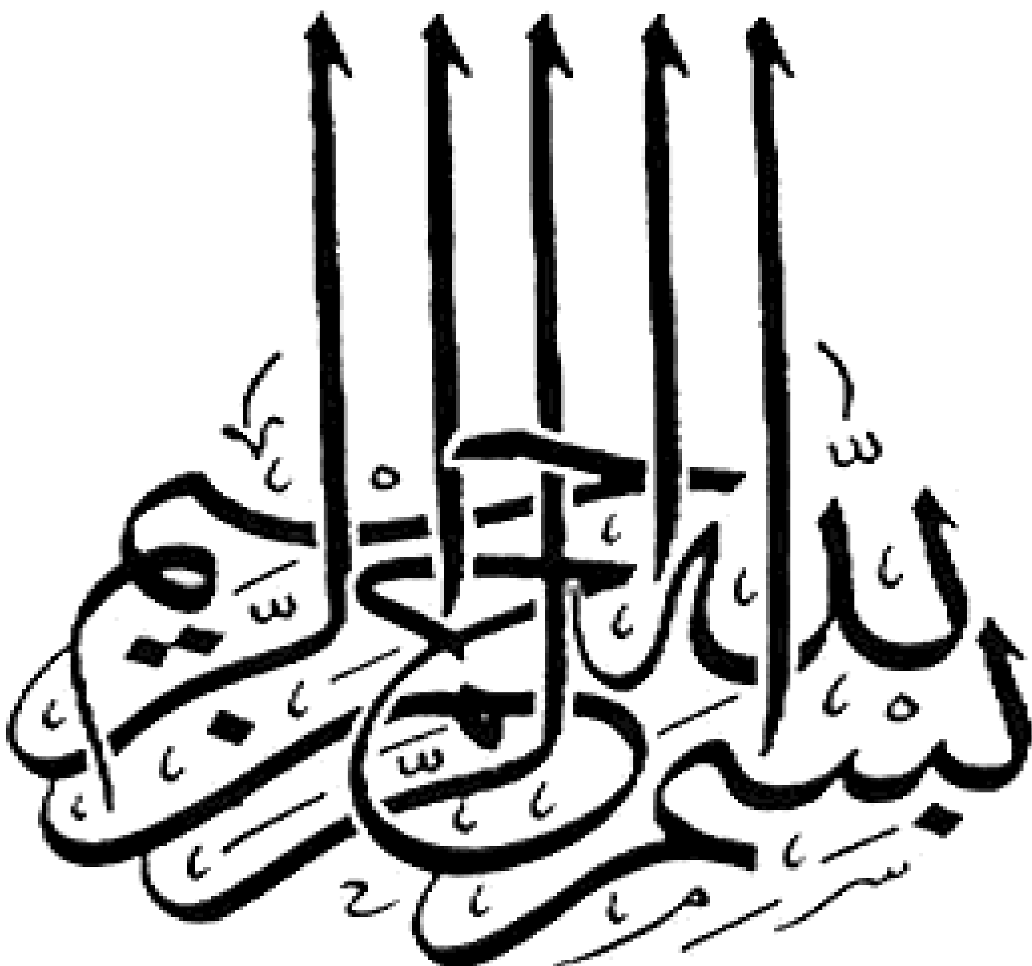
بسم الله الرحمن الرحيم

ACKNOWLEDGEMENT

All praise is to Allah the Almighty the creator of the universe. Who blessed me with the gleaming mind, and enabled me to successfully complete my research work. All regards to the prophet Mohammad (S.A.W) who paved us to the right path with quintessence of faith in Allah.

It is not a formality but the emotional association to acknowledge the person who has helped me to achieve this goal. I would like to gratefully acknowledge my supervisor **Dr. Muhammad Islam**, Assistant Professor School of Chemical & Materials Engineering (SCME) National University of Sciences and Technology (NUST) Islamabad, who truly made a difference in my life. It was under his tutelage that I developed a focus and became interested in Material Science. He provided me with direction, technical support and became more of a mentor and friend, than a professor. I doubt that I will ever be able to convey my appreciation fully, but I owe him my eternal gratitude.

I gladly express my regards to respected **Dr. Umair Manzoor** Assistant Professor Department of Physics COMSATS University Islamabad for his co-supervision, guidance and relentless technical discussions. I would like to express my sincere thanks to **Dr. Muhammad Shahid, HOD** Material Engineering for his sincere and inspire guidance and for technical assistance.

I greatly acknowledge **Dr. Mohammad Mujahid Principal& Dean** School of Chemical and Materials Engineering (SCME), NUST for providing a platform to utilize my skills in the research work. It is my pleasure to appreciate and thank Dr. Mohammad Bilal Khan, for his inspiring way of teaching and guiding. I feel honor to acknowledge Dr. A. Q. Malik Head of Chemical Engineering Department for providing the laboratory facilities. I would also like to thank all the faculty members, non-teaching staff and my fellow students for the help provided to me at the various stages.

I am thankful to my project fellows and friend Shahzad Slam, Asif Mehmood, Mehboob Alam, Asad Hameed and Nasir Mehmood who were very kind to me and who motivated me towards research. I would never forget his friendship and company that was the real source of motivation and encouragement. I am grateful to my friends and class fellows, Aftab Akram (Phd scholar), Mujtaba Ikram, Irshad Ul Haq (NCVI), Mohammad Faheem (NCVI), Saqib Khan (SEECS), Sibghat Ullah (IGIS), Adil Qayum being the surrogate family at NUST and for providing the company and support.

I specially acknowledge Rector NUST Mohammad Asghar for his countless efforts to make SCME and NUST one of the prestigious institution in Pakistan.

I have no words to express my feelings and gratitude for my dignified father and my loving mother to whom I owe all that I have in my life. All that I have is due to her prayers. I am indebted to my parents and the whole family for their moral support and encouragement when it was most required.

Majid Khan

Dedicated to my

Loving Parents

& family

ABSTRACT

Molybdenum (Mo) is a commonly used back contact material for CIGS-based $Cu(In,Ga)Se_2$ thin films solar cells. Numerous properties are required for Mo to play better role as back contact material including chemical and mechanical inertness during deposition process, high conductivity, an appropriate thermal expansion coefficient with contact layers and low contact resistance with the $Cu(In,Ga)Se_2$ layer. Mo thin films were deposited on well-cleaned soda-lime glass substrates using DC-plasma magnetron sputtering. In the design of experiment deposition was optimized for maximum beneficial characteristics by monitoring effect of process variables such as deposition power (100-200W), Ar pressure (0.002-0.0123mbar) and substrate temperature (23-400^{0}C). Their electrical, structural and morphological properties were analyzed to study the effect of these variables. The electrical resistivity of Mo thin films could be reduced either by increasing the deposition power and substrate temperature or by decreasing the Ar pressure. Within the range of analyzed deposition parameters, Mo thin films showed a mono-crystalline nature and the crystallites were found to have an orientation along [110] direction. The surface morphology of thin films showed that a highly dense microstructure has been obtained. The surface roughness of films increased with substrate temperature and deposition power. The adhesion of Mo thin films could be improved by increasing the Ar pressure and deposition power. Atomic force microscopy was used for the topographical study of the films and to determine the roughness of the films. X-ray diffractrometer (XRD) and scanning electron microscopy (SEM) analysis were used to investigate the crystallinity and surface morphology of the films. Hall Effect Measurement System was used to find resistivity, carrier mobility and carrier density of deposited films. The adhesion test was performed using scotch hatch tape adhesion test. Mo thin films prepared at deposition power of 200W, substrate temperature of 400^{0}C and Ar pressure of 0.002mbar exhibiting a mono-crystalline structure with an orientation along (110) direction, thickness equal to 1μm and electrical resistivity equal to $7.02\times10^{-05}\Omega$cm was obtained.

Keywords: Mo thin films; DC-plasma magnetron sputtering; Mono-crystalline

Table of Contents

ACKNOWLEDGEMENT iii

DEDICATION v

ABSTRACT vi

CHAPTER NO 1

1.1 INTRODUCTION 2

1.2 THE RESEARCH OBJECTIVE 4

1.3 OUTLINE OF THE THESIS 4

CHAPTER NO 2

2.1 INTRODUCTION 7

2.2 DEPOSITION PROCESSES 7

2.2.1 Selection Criteria for a Particular Deposition Process 9

2.3 CHEMICAL VAPOR DEPOSITION (CVD) 11

2.4 PHYSICAL VAPOR DEPOSITION (PVD) 11

2.4.1 Thermal Evaporation Deposition 12

2.4.2 Ion plating 14

2.5 PHYSICS OF SPUTTERING 15

2.5.1 Introduction 15

2.5.2 Sputtering Mechanism 16

2.5.3 Sputtering Yield 18

2.5.4 Sputtering Configurations 20

2.5.4.1 DC-Plasma Sputtering 21

2.5.4.2 RF-Plasma Sputtering 22

2.5.5 Magnetron Sputtering 23

2.5.5.1 The Planar Magnetron 24

2.5.5.2 Magnetron Operation 26

2.5.5.3 Balanced and Unbalanced Magnetron Sputtering 27

2.5.6 Reactive Sputtering 28

2.6 PROPERTIES OF PVD THIN FILMS 29

2.6.1 Processes of Formation of Thin Film 29

2.6.1.1 Condensation 30

2.6.1.2 Nucleation and Growth 30

2.6.2 Microstructure Evolution-Structure Zone Model (SZM) 32
2.6.3 Electrical Properties 35
2.6.3.1 Resistivity and Sheet Resistance 35
2.6.3.2 Temperature Coefficient of Resistivity (TCR) 37
2.6.4 Optical Properties 37

CHAPTER NO 3
3.1 INTRODUCTION 42
3.2 CIGS THIN FILM SOLAR CELL TECHNOLOGY 43
3.2.1 Introduction 43
3.2.2 Device Structure 45
3.3 THIN FILMS FOR BACK CONTACT 46
3.3.1 Molybdenum Thin Films 46
3.3.2 Features of Molybdenum Thin Films 47
3.3.2.1 Electrical properties of Mo thin films 48
3.3.2.2 Stresses in Molybdenum Thin Films 49
3.3.2.3 Adherence of Molybdenum Thin Films with the Substrate 50
3.3.2.4 Molybdenum Bilayer Process 51
3.3.2 Other Materials Used as Back Contact 51

CHAPTER NO 4
4.1 EXPERIMENTAL PROCEDURE 55
4.1.1 Substrate Preparation 55
4.1.2 DC-Magnetron Sputtering 55
4.2 CHARACTERIZATION TECHNIQUES 57
4.2.1 Scanning Electron Microscope (SEM) 57
4.2.2 Atomic Force Microscope (AFM) 58
4.2.3 X-Ray Diffraction (XRD) 59
4.2.4 Electrical Characterization 60
4.2.4.1 Four Point Probe Method 60
4.2.4.2 Hall Effect Measurement System 61
4.2.5 Scotch Tape Test 61

CHAPTER NO 5

5.1 STUDY OF MOLYBDENUM SPUTTERED THIN FILMS 64

5.2 ARGON PRESSURE.. 64

5.3 DEPOSITION POWER 71

5.4 SUBSTRATE TEMEPERATURE 75

CHAPTER NO 6

6.1 CONCLUSIONS.. 81

6.2 FUTURE RECOMMENDATIONS 82

CHAPTER No 1

INTRODUCTION

1.1 INTRODUCTION

Thin film and devices play a vital role in the development of modern science. Thin film is a two dimensional form of solid material, whose one dimension, called the thickness, is much smaller than the other two dimensions. It is formed by atom to atom or molecule to molecule condensation process. In technical terms, the thickness of the films must be restricted to the order of mean free path of the carriers contributing in the particular electronic transport process for which the film has been fabricated. The maximum thickness may vary from a nanometer to a few micrometers depending upon the field of application [1].

The development of thin film technology has sets its application in different fields from microelectronics to optics, space science to aircrafts, superconductivity to photovoltaics. One of the most important applications of thin films is in the photovoltaic devices and solar cells applications [2-3]. In the photovoltaic devices, the use of thin films permits not only material costs saving but also the production of large area devices at a relatively low cost. Hence in addition to major effect to diversity of new and future scientifically based technology, the thin films studies have directly or indirectly caused the improvement of many new areas of research in solid state physics and chemistry and will continue to play ever more important roles in the study of a many of problems of basic and scientific importance.

Thin films play an important role in today's World energy crises. Therefore main research is ongoing on thin films solar cells to improve its performance and make it cost effective. Most of the compound thin film semiconductor solar cells are direct band gap semiconductors. Therefore the absorption of sunlight occurs within a few microns. Thin film solar cells are classified as amorphous silicon, CdTe and $CuInSe_2$ and its alloys. CIGS has been reported as the maximum efficient thin film solar cell. The device structure of CIGS solar cell consists of back contact layer, p-type absorber layer, buffer layer and top contact layer or window layer.

The back contact layer is a type material at the bottom of absorber layer whose role is to collect charge carriers and provide them to the external circuit. In most of the standard cells the requirements of a back contact material are to have low resistivity, not to stop the flow of majority carriers such as holes and to permit the diffusion of sodium from substrate to absorber layer in CIGS solar cells. Molybdenum (Mo) is the descent choice and is mainly used as a back contact (BC) material in copper indium gallium di-selenide (CIGS) thin films solar cells. Various properties are required for Mo to play a better role as a back contact materials including chemical and mechanical inertness during deposition process, high conductivity, an appropriate thermal expansion coefficient with contact layers and low

contact resistance with the $Cu(In,Ga)Se_2$ layer. Efficiencies greater than 19% have been reported for this type of devices fabricated using Mo films acting as an ohmic contact, deposited by conventional RF- magnetron sputtering [4].

Sputter deposited thin films of molybdenum (Mo) are progressively more being used as the gate electrode in GaAs-based metal gate field effect transistors (MESFETs) and silicon-based metal–oxide semiconductor (MOS) devices [5-8], because of its low resistivity and high melting point. Successful performance of Mo as the gate electrode was found to be affected by the deposition conditions.

There are many requirements desirable for a good back contact (BC) material to be used in $Cu(In,Ga)Se_2$ (CIGS) solar cells. A certain inertness of the contact material is necessary for reproducible CIGS absorber growth in the highly corrosive process atmosphere during the CIGS deposition. The contact layer must function as barrier that holds back diffusion of impurities from the substrate into the absorber. For good electronic device properties, the formation of an ohmic contact for the majority carriers (holes) from the p-type CIGS and a low recombination rate for the minority carriers (electrons) at the CIGS/BC interface is needed. Finally, a high optical reflectance is necessary to minimize optical losses. Therefore Mo fulfills most of the requirements. It is inert during the deposition, allows for the growth of large grains, and forms an ohmic contact through an intermediate $MoSe_2$ layer [9].

Thin films of Mo have been prepared on different types of substrates, such as soda lime glass, borosilicate glass and polymeric flexible substrate, using sputtering and e-beam evaporation. Because of the presence of a plasma, sputtering exhibits added benefits in the deposition process for many thin film technologies. Sputtering has better step coverage than evaporation as the ad-atoms have higher surface diffusion energy. The sputtering process is also much better at producing layers of compound materials and alloys and in controlling the microstructure and phase of the deposit. An extensively used sputtering technique for Mo thin films is DC-magnetron sputtering where a magnetic field is superimposed on the electric field. This leads to electron confinement near the target resulting in higher ionization of the sputtering gas, and consequently, higher deposition rates are obtained. The physical properties of the deposited films are mainly affected by the deposition parameters such as working pressure, deposition power, deposition time, and target to substrate distance, thickness of the film and substrate temperature.

1.2 THE RESEARCH OBJECTIVE

The objective of this work is to prepare Mo thin films to be used as efficient back contact materials and utilize characterization techniques for the investigation of the growth as wells the physical properties of Mo thin films deposited through DC-plasma magnetron sputtering on soda lime glass substrate.

The high efficiency Cu(In,Ga)Se_2 solar cell results so far have been reported on Mo back contact layers prepared by DC-magnetron sputtering [9]. So this is the choice of deposition technique to deposit thin films. Various process variables were selected to find an appropriate condition to deposit thin films of Mo required for CIGS solar cell.

The effects of process parameters, such as Ar pressure, deposition power and substrate temperature, on the properties of the deposited films have been studied. These process parameters were optimized to get high conductivity Mo thin films to be used in CIGS solar cell as a back contact. The surface morphology of the Mo films is to be investigated by scanning electron microscopy (SEM) and atomic force microscopy (AFM) while the crystallinity of thin films will be investigated by X-ray diffraction (XRD) analysis. The compositional analysis fabricated Mo films is to be done by energy dispersive X-ray (EDX). The carrier's concentration and mobility as well as resistivity of the films will be investigated by Hall Effect measurement system. The results obtained will be correlated with the structural properties of Mo thin films.

1.3 OUTLINE OF THE THESIS

Chapter No.1 provides the brief introduction that includes the objective of the present work.

Chapter No.2 described the Physical vapor deposition techniques for fabricating thin films. Types of PVD techniques and the physics behind each type of PVD techniques are discussed in detail. Formation of thin films and microstructural evolution (Structure Zone Model) behind the PVD techniques are also described in this chapter. At the end of this chapter the electrical and optical properties of thin films fabricated through PVD techniques are summarized.

Chapter No.3 present comprehensive and corroborative studies of molybdenum back contacts, which have been used in Cu(In,Ga)Se2 solar cells. This chapter discusses in detail the properties of Mo thin films, literature survey on back contact materials and current state of research on Mo thin films.

Chapter No.4 presents the experimentation performed in the present work to deposit Mo thin films through DC-plasma magnetron sputtering and various characterization tools to analyze the films.

Chapter No.5 presents the results obtained in this work and the related discussion.

Finally, Chapter No.6 summarizes conclusions drawn from this work and provides suggestions for future directions and work improvements.

References

[1] K. L. Chopra; Thin Film Phenomena; Robert E. Krieger Publishing Company,Huntington, New York (1969).

[2] L. I. Maissel and R Glang (eds); Hand Book of Thin Film and Technology, Mc Graw Hill Com., New York, 1970.

[3] K. L. Chopra and L. K. Malhotra, “Thin Film Technology and Applications”, (Tata-Mc-Graw Hill, New Delhi). (1985)

[1] M.A. Contreras, B. Egaas, K. Ramanathan, J. Hiltner, A. Swartzlander, F. Hasoon, and R. Noufi, Progress toward 20% efficiency in Cu(In,Ga)Se_2 polycrystalline thin-film solar cells, Progress in Photovoltaics Research and Applications 7 311–316 (1999)

[2] T.T. Bardin, J.G. Pronko, R.C. Budhani, J.S. Lin, R.F. Bunshah, The effects of oxygen concentration in sputter deposited molybdenum films, Thin Solid Films 165 243–247 (1988)

[3] L. Krusin-ElBaum, M.O. Aboelfotoh, T. Lin, K.Y. Ahn, Transport in refractory metals and their interaction with SiO2: comparison of tungsten and molybdenum, Thin Solid Films 153 349–358 (1987)

[4] J.S. Lin, R.C. Budhani, R.F. Bunshah, Effects of substrate bias on the resistivity and microstructure of molybdenum and molybdenum silicide films, Thin Solid Films 153 359–368 (1987)

[5] T. Yamaghuchi, R. Miyagawa, Effects of oxygen on the properties of the sputtered molybdenum thin films, Japanese Journal of Applied Physics V30 (9A) 2069–2073 (1991)

[6] T. Wada, N. Kohara, T. Negami and M. Nishitani. Jpn, Chemical and structural characterization of Cu(In, Ga)Se_2/Mo interface in Cu(In, Ga)Se_2 solar cells, J. Appl. Phys. **35,** 1253-1256 (1996)

[7] G. Gordillo, F. Mesa, C. Caldero´ n, Electrical and morphological properties of low resistivity Mo thin films prepared by magnetron sputtering, Brazilian Journal of Physics V36 (3B) 982–985(2006)

[8] A. E. Hady B. Kashyout, Hesham M.A. Soliman, Hanaa A. Gabal, P. A. Ibrahim, M. Fathy, Preparation and characterization of DC sputtered molybdenum thin films, Alexandria Engineering Journal 50, 57–63(2011)

[9] J. H. Scofield, A. Duda, D. Albin, B. L. Ballard, P. K. Predecki,“Sputtered molybdenum bilayer back contact for copper indium diselenide based polycrystalline thin–film solar cells.” Thin Solid Films 260, 26-31(1995)

CHAPTER NO 2

Physical Vapor Deposition (PVD) Techniques for Thin Films

2.1 INTRODUCTION

Physical vapour deposition is one of the various coating techniques available nowadays to surface engineers. It is used to deposit films and coatings or self-supported shapes such as sheet, foil, and tubing.It is particularly popular for adding traditional coatings of CrN, TiC and TiN onto a variety of bulk materials such as tool steels. The researchers and industrial interest on this process was greatly increased when a large increase in tool life of high speed steel tools PVD coated with TiN or TiC was demonstrated. PVD techniques are now used for a variety of applications, from decorative to utilitarian over significant segments of the engineering, chemical, nuclear, microelectronics and related industries.

As the name implies, PVD is a vapour deposition process. Thus one or more of the depositing materials is vaporised from the condensed phase and is subsequently allowed to condense onto an atomically cleaned substrate. The vapor-phase material can consist of ions or plasma and is often chemically reacted with gases introduced into the vapor, called reactive deposition, to form new compounds. This is followed by film nucleation and growth. The basic PVD processes are evaporation, sputtering and ion plating. Materials are physically created in the vapor phase by energetic bombardment of a source (e.g. sputtering target) and subsequent ejection of material. Because of the presence of a plasma, sputtering exhibits added benefits in the deposition process for many thin film technologies. PVD was first discovered in 1852, and was developed as a thin film deposition technique by Langmuir in the 1920s. It has better step coverage than evaporation as the adatoms have higher surface diffusion energy. The sputtering process is also much better at producing layers of compound materials and alloys and in controlling the microstructure and phase of the deposit. A widely used sputtering technique is dc magnetron sputtering where a magnetic field is superimposed on the electric field. This leads to electron confinement near the target resulting in higher ionization of the sputtering gas, and consequently, higher deposition rates are obtained. A number of specialized PVD processes have been derived from these processes and extensively used, including reactive ion plating, reactive sputtering, unbalanced magnetron sputtering, HPPMS, and filtered cathodic arc deposition.

2.2 DEPOSITION PROCESSES

In general, deposition processes may principally be divided into two types [1]:

1. Processes involving droplet transfer such as plasma spraying, arc spraying, wire-explosion spraying, and detonation gun coating

2. Those Processes involving an atom-by-atom transfer mode such as the PVD processes of evaporation, ion plating and sputtering, chemical vapor deposition (CVD), and electrodeposition.

The chief disadvantage of the droplet transfer process is the porosity in the final deposit, which affects the properties.

There are three steps in the formation of any deposition process:

1. Synthesis of the material to be deposited: (a) transition from a condensed phase (solid or liquid) to the vapor phase (b) for deposition of compounds, a reaction between the components of the compound, some of which may be introduced into the chamber as a gas or vapor.
2. Transport of the vapors between the source and substrate.
3. Condensation of vapors (and gases) followed by film nucleation and growth.

Table 2- 1: Comparison of thin film deposition methods [2]

Technique	Advantages	Disadvantages
Sputtering	Dense films Good uniformity Wide range of inorganic materials	relatively slow
Thermal Evaporation	Fast Relatively simple	Limited range of materials Low density films without ion or plasma assist
e-Beam Evaporation	Fast Wide range of inorganic materials	high voltages
CVD	Gives good control of coating chemistry Multidirectional deposition Uniform distribution over large areas	Mostly involve safety and contamination High cost for compounds with sufficient purity Difficult to scale Often uses hazardous liquids or gases

There are significant differences between the various atom transfer processes. In CVD and electrodeposition processes, all of the three steps mentioned above take place simultaneously at the substrate and cannot be independently controlled. Thus, if a choice is made for a process parameter such as substrate temperature (which governs deposition rate in CVD), one is stuck with the resultant microstructure and properties. On the other hand, in the PVD processes, these steps (particularly steps 1 and 3) can be independently controlled and one can therefore have a much greater degree of flexibility in controlling the structure and properties, and deposition rate. This is a very important consideration. These techniques have their own advantages and disadvantages that are given in the Table 2-1.

2.2.1 Selection Criteria for a Particular Deposition Process

The selection of a particular deposition process depends on several factors:

- material to be deposited
- limitations imposed by the substrate, e.g. material, size, temperature stability
- specific application
- deposition rate
- adhesion of film to substrate
- throwing power
- purity of source material
- apparatus required and availability of same
- cost
- safety considerations, e.g. toxicity
- process stability
- manufacturing considerations, e.g. batch size, throughput, process controls
- abundance of source materials

The selection criteria for each deposition process are given in the Table 2-2, so that on can select a suitable deposition process. Usually one process cannot meet all of the above requirements and more than one technique can be used to deposit a given material. As a result, hybrid processes are now being used to deposit many thin film materials. Evaluation of each process for the specific application will help lead to a rational choice of deposition process or hybrid process.

Table 2- 2: Criteria for selecting deposition processes [3]

	Evaporation	Ion Plating	Sputtering	Cathodic Arc Deposition	Chemical Vapor Deposition	Polymer Deposition	Electrodepositon	Thermal Spraying
Mechanism of production of depositing species	Thermal Energy	Thermal Energy	Momentum Transfer	Thermal Energy	Chemical Reaction	Thermal Energy	Solution	Flames of Plasmas
Deposition rate	Up to 750,000 Å/min	Up to 250,000 Å/min	Low except for pure metals and dual magnetron	Can be very high	200-2500 Å/min	100,000 Å/s	Low to high	Very high
Deposition species	Atoms & ions	Atoms & ions	Atoms & ions	Ions	Atoms	Monomers/polymers	Ions	Droplets
Throwing power	Poor	Good	Good	Good	Good	Good	Good	No
Metal deposition	Yes	Yes	Yes	Yes	Yes	No	Yes, limited	Yes
Alloy deposition	Yes	Yes	Yes	Yes	Yes	No, but molecular doping possible	Quite limited	Yes
Refractory compound deposition	Yes	Yes	Yes	Yes	Yes	No	Limited	Yes
Energy of deposited species	Low	Can be high (~0.1-0.5 eV)	Can be high (1-100 eV)	Can be high (1-100 eV)	Can be high with plasma assisted CVD	Low	Can be high	Can be high
Bombardment of substrate	Generally no	Yes	Yes or no depending on geometry	Yes	Possible with PECVD	No	No	Yes
Substrate heating (by external means)	Yes, normally	Yes or no	Yes or no	Yes or no	Yes	No, cooling generally required	No	Not normally

2.3 CHEMICAL VAPOR DEPOSITION (CVD)

Chemical vapor deposition (CVD) is a widely used materials-processing technology. The majority of its applications involve applying solid thin-film coatings to surfaces, but it is also used to produce high-purity bulk materials and powders, as well as fabricating composite materials via infiltration techniques. CVD involves a precursor gas or gases flowing into a chamber containing one or more heated objects to be coated. Chemical reactions occur on and near the hot surfaces, resulting in the deposition of a thin film on the surface. This is accompanied by the production of chemical by-products that are exhausted out of the chamber along with un-reacted precursor gases.

This method is used to produce high-purity, high-performance solid materials. The process is often used in the semiconductor engineering to produce thin films. In a typical CVD process, the substrate is exposed to one or more unstable precursors, which react and/or decompose on the substrate surface to produce the desired deposit. As would be expected with the large variety of materials deposited and the wide range of applications, there are many variants of CVD. It is done in hot-wall reactors and cold-wall reactors, at sub-tor total pressures to above-atmospheric pressures, with and without carrier gases, and at temperatures typically ranging from 200-1600°C. There are also a variety of enhanced CVD processes, which involve the use of plasmas, ions, photons, lasers, hot filaments, or combustion reactions to increase deposition rates and/or lower deposition temperatures. There are also many derivatives of the CVD terminology, such as metal-organic chemical vapor deposition (MOCVD) or, less commonly, organo-metallic chemical vapor deposition (OMCVD), which are sometimes used to note the class of molecules used in the deposition process.

Here we will focus only on the physical vapor deposition process.

2.4 PHYSICAL VAPOR DEPOSITION (PVD)

Physical Vapor Deposition (PVD) is a physical process in which a target material is evaporated or sputtered to deposit it on substrate surface.

The term PVD stands for Physical Vapor Deposition and one of the techniques used for growing thin films. It is an atomistic deposition process in which material is vaporized from a solid or liquid source in the form of atoms or molecules. The vapors are then transported through a vacuum or low pressure gaseous (plasma) environment to the substrate

where it condenses. PVD is basically a surface science process. It has three basic steps to deposit a thin film.

1. Sublimate solid state of target material to vapor state.
2. Atoms or molecules or ions in vapor state passing through the vacuum space to the surface of substrate.
3. Deposit target material on the surface of substrate to form a desired thin film.

PVD process can be used to deposit thin films of elements, alloys and compounds. Compounds thin films can be formed through reactive deposition process, in which the depositing material is deposited with the ambient gas environment such as nitrogen (e.g. AlN, TiN).

Different physical techniques are used in PVD method. Each technique can be divided into more sub-techniques which apply different mechanisms to achieve its goal. The main categories of PVD processing are

A. Thermal Evaporation Deposition
   i. Resistive Heating
   ii. Laser Deposition
   iii. Arc Deposition
   iv. Electron Beam Gun Evaporation
   v. RF- Heating
   vi. Molecular Beam Epitaxy, MBE
B. Plasma Sputtering Deposition
   i. Planar Diode Sputtering Deposition (DC Sputtering Deposition)
   ii. RF Sputtering Deposition
   iii. Dual Cathodes Sputtering Deposition
   iv. Triode Sputtering Deposition
   v. Magnetron Sputtering Deposition
C. Ion Plating

2.4.1 Thermal Evaporation Deposition

Evaporative PVD processes are processes where the vaporization of the coating material is obtained by heating the condensable material to evaporation. It is also called Vacuum deposition process. In this process, heat is input into the source material (often called the charge) to create a plume of vapor which travels in straight-line paths to the substrate. Upon arrival at the substrate, the atoms, molecules, and clusters of molecules

condense from the vapor phase to form a solid film. The heat of condensation is absorbed by the substrate. Evaporation is normally carried out in a pressure range of 13 to 0.013mPa or 10^{-5}Torr to 10^{-9}Torr. Under these conditions, the evaporated atoms undergo a collision-less line of sight transport before condensing on the substrate. To assure that the coating thickness on the substrate is even, planetary substrate holders are sometimes used. A gas such as argon is sometimes introduced to scatter the vapor flux and a more uniform thickness results. In some processes a reactive gas is introduced to react with the vapor flux and the desired compounds are synthesized.

Different methods for heating the source are resistive heating, electromagnetic induction heating and electron beam heating which is shown in the schematic above. In the latter the evaporation is accomplished by the bombardment of the condensable material with a beam of accelerated electrons. An advantage over other PVD processes is that it can be used at very high evaporation temperatures, and thus even refractory materials and ceramics can be vaporized.

Figure 2-1 shows the schematic of electron beam evaporation system. The thickness of the deposit is greatest directly above the center of line source and decrease away from it.

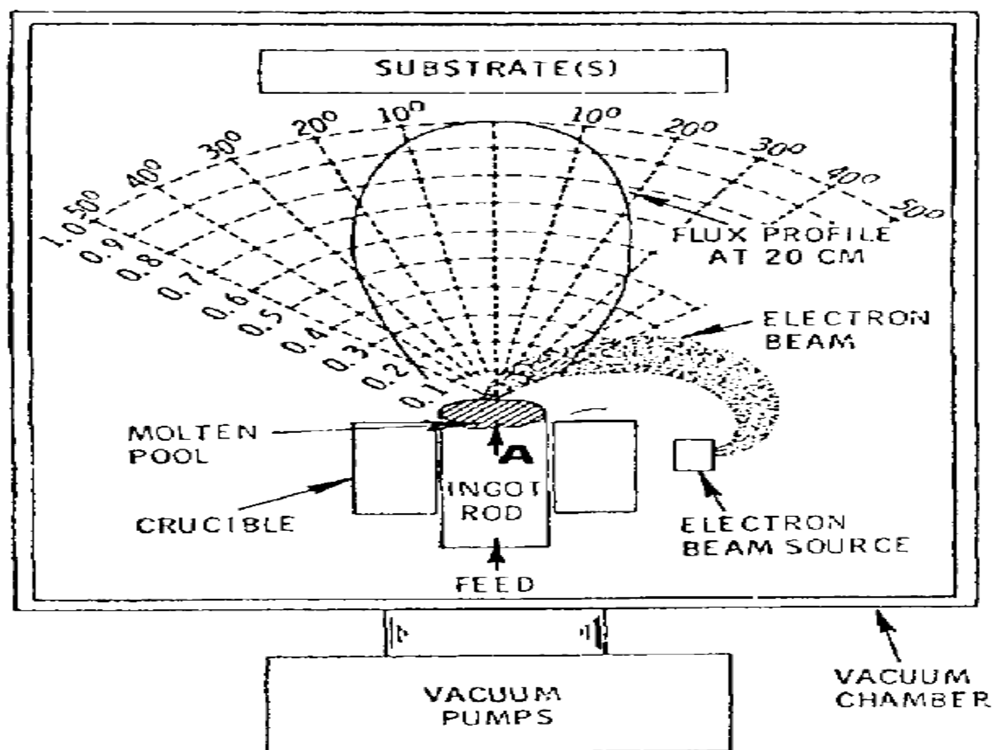

Figure 2-1: Schematic of vacuum-evaporation process using electron beam heating [3].

2.4.2 Ion plating

Ion plating is a hybrid process. The term ion plating is a generic term applied to atomistic film deposition process in which the substrate surface and the growing film are subjected to a flux of energetic bombarding particles sufficient to cause changes in the film formation process and the properties of the deposited film.

Ion implantation is involved with the alteration of the substrate surface and near surface regions. It is mainly a low temperature process capable of creating non-equilibrium alloys and compounds in the surface. Smoothness, dimensional tolerances, and temper are totally unaffected. The implant is an integral part of the substrate and due that there is no sharp interface the implanted layer cannot peel off. This process is expensive and provides a shallow protective layer. Ions are embedded into the material by the virtue of their kinetic energy, provided by the electrical acceleration, to a depth determined by the energy loss within the substrate typically varying from 0.1 to 0.8μm at low temperatures.

Figure 2-2 shows the schematic of ion plating configuration. Early work shows us that ion plating was concerned with the deposition of atoms from a source of thermal evaporation or sublimation and also from sputtered ion plating. Bombardment was by ions extracted from plasma by applying a negative potential to the surface to be coated which was immersed in the plasma.

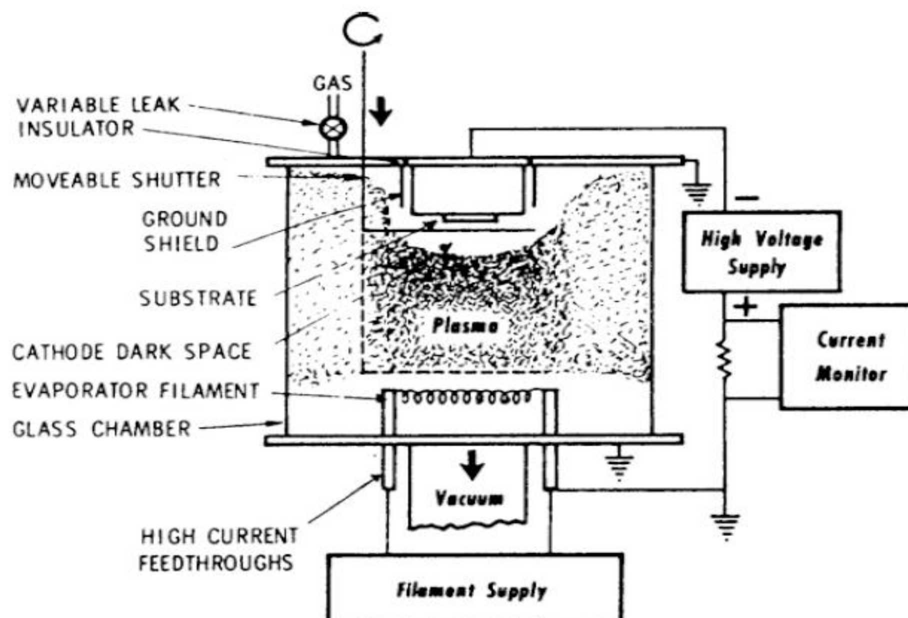

Figure 2-2: An ion plating configuration using a DC diode discharge and a thermal vaporization source [3].

Recently the term ion plating is mainly concerned with processes where the surface to be coated is in contact with a plasma and the term ion assisted deposition (IAD) or ion beam enhanced deposition (IBED) is used where the substrate is bombarded by an ion beam in a vacuum environment during deposition.The emergence of Ion-Assisted Coatings (IAC or IBAD) is the result of the combination of two surface technologies namely, vacuum deposition and ion implantation. Thus unlike ion implantation IBAD produces a coating. The ion beam provides a controlled way for supplying energy in the film and substrate to improve film growth and adhesion and to modify the initial substrate surfaces, the coating itself, its composition and microstructure. As in ion implantation, the ion beam is used to create materials often outside the bounds of normal phase equilibrium and to produce surface modifications in a controlled and reproducible manner.

2.5 PHYSICS OF SPUTTERING

2.5.1 Introduction

The physical process that we now call sputtering was first reported in 1852 by Sir William Robert Grove [1], who described the effect as cathode disintegration. Grove’s apparatus utilized a cathode made of silver-coated copper, but his manually pumped vacuum was insufficient that the world’s first sputter deposited film was probably not silver, but silver oxide.

In 1921, Sir. John Thomson renamed this phenomenon which refers to the rapid ejection of small particles from a cathode as ‘frying bacon splutters fat’ to spluttering. In a scientific paper two years later, Thomson dropped ‘l’ from spluttering in favors of a less common variation and it has been sputtering even since.

Subsequent investigation led to an understanding of the basic physics of the sputtering and resulted in a variety of industrial coating application as metal films for mirror (1875) or gold film deposition on wax photograph masters (1930). When sputtering was nearly 100 years old, the first microelectronics device – the solid state transistor - was demonstrated publicly in 1948 and since that time thin film deposited by sputtering - i.e. by physical vapor deposition (PVD) has become an essential part of integrated circuit fabrication technology.

In the 1970s, sputtering began to displace hot filament evaporation because DC magnetrons were capable to deposit high quality aluminum alloys at deposited rates and costs comparable to evaporation together with better control of film composition and better step coverage.

There is a wide variety of sputtering techniques that are currently used to deposit thin films for use in magnetic storage media (cassette tapes, computer discs), optical thin films and micro-circuits.

2.5.2 Sputtering Mechanism

It is relatively simple process in which an energetic particle bombards a target surface with sufficient energy to eject one or more atoms from the target (Figure 2-3). In this process the substance to be deposited (target) is kept in the form of an electrode (whose surface atoms (or molecules) are ejected by momentum transfer from the bombarding ions. The ejected or sputtered atoms are allowed to condense on a substrate to form a thin film. If the ejection is due to bombardment by positive ion, the process is known as cathodic sputtering. Sputtering process is statistical in nature which occurs as a result of a momentum-exchange collisional cascade process initiated near the target surface by an incident energetic projectile. The most commonly used incident species are inert gas ions (e.g. Ar+, Kr+, Xe+), but sputtering can also result from the bombardment of other energetic ions, neutrals, electrons and even photons. In general, the physical effect caused by bombardment with a neutral or an ion of the same species and energy will be identical. The ion is usually neutralized by pulling an electron from the near surface region just prior to impact, and so it impacts the surface as a neutral. Because it is quite easy to generate large fluxes of ions at controlled energies all applications of sputtering use ions as the bombarding particles.

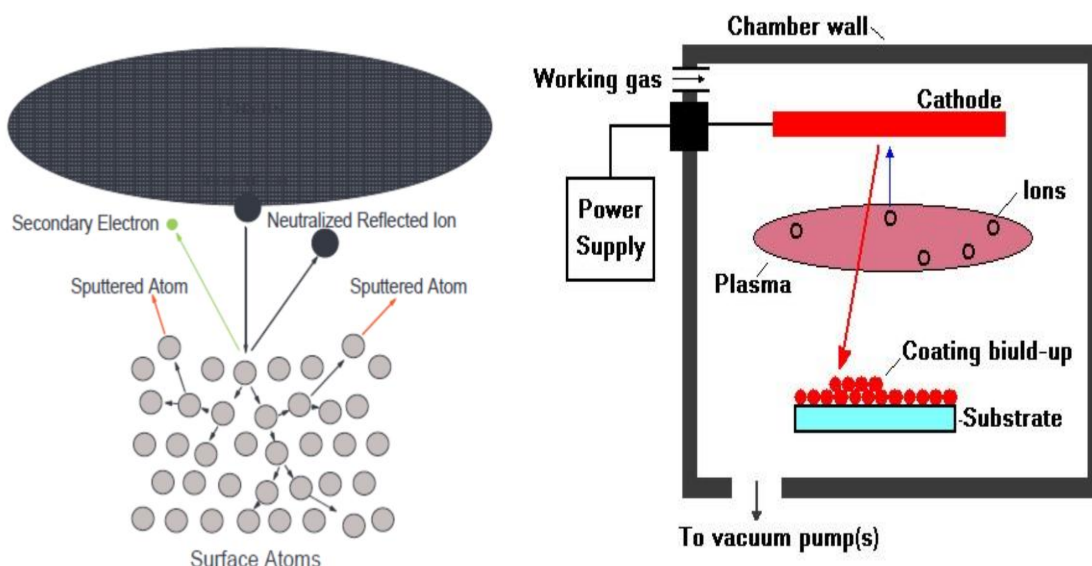

Figure 2-3: Schematic illustration of physical sputtering process [4].

Two theoretical models have been proposed for sputtering:

1. In first theory the surface of the target is heated enough to be vaporized to due to the bombardment of energetic ions. This theory was named as thermal vaporization theory.
2. In the second theory the surface atoms of the target material are emitted when kinetic moments of incident particles are transferred to target surface atoms. This theory was so called momentum transfer theory.

Nowadays the theory of collision cascade in the surface layer of the solid is to be believed. Let us discuss the how the momentum transfer occurs between the sputtering species. As the target material is bombarded by ions the momentum exchange transfer occurs. To elaborate this momentum exchange transfer, consider a particle of mass $M_i$and velocity V_i which impacts on a line of centers with a target particle of mass M_t that is initially at rest, as shown in figure

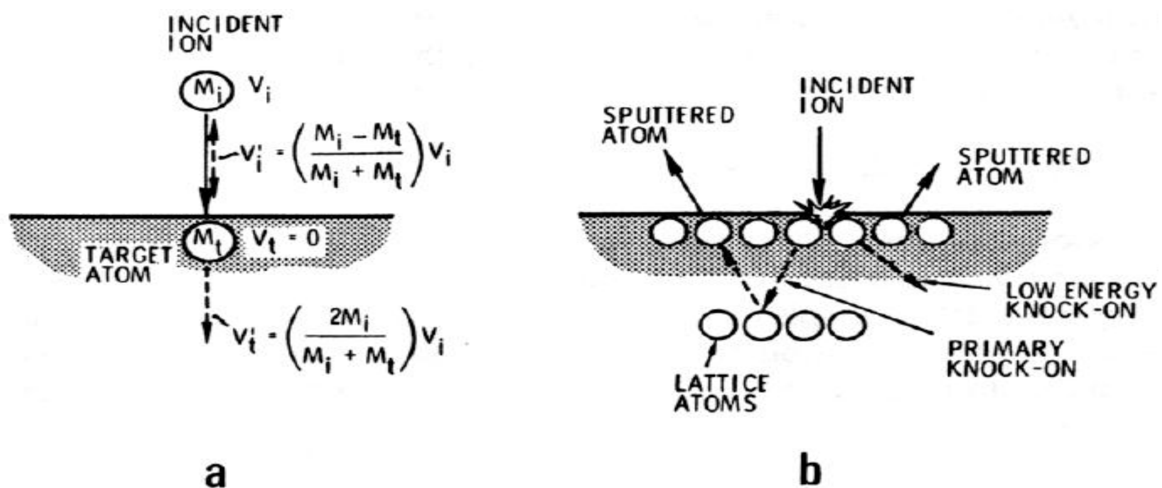

Figure 2-4: Schematic diagram showing momentum exchange processes that occur during sputtering; M_i and V_i are the ion mass and velocity, M_t and V_t are the target-atom mass and velocity, and the prime superscript denotes velocities after collision [5].

The following three simple observations can be obtained from the momentum exchange transfer.

1. The momentum imparted to the target particle drives it into the lattice.
2. From a simple line-of-centers atomic collision calculation, a fraction

$$\varepsilon = \frac{4M_iM_t}{(M_i+M_t)^2} \quad \text{Equation 2-1}$$

of the kinetic energy of the incident particle is transferred to the target particle. Where ε is the energy transfer coefficient.

3. The expression of the sputtering yield can be derived by assuming perpendicular ion incidence onto a target consisting of a random array of atoms (a good approximation for a small grain polycrystalline material) with a planar surface.

$$\gamma = (\text{constant})\varepsilon\frac{E}{U}\alpha(M_t/M_i)$$

Where E is the energy of the incident ion, U is the heat of sublimation for the target material and the term$\alpha(M_t/M_i)$ is a near linear function of(M_t/M_i).

The yield is directly dependent on the energy transfer coefficientε. The mass dependence of $\varepsilon\alpha$ does not varies greatly from one material to another. The primary material-sensitive factor is the heat of sublimation, and this is only a first power dependence. This is in contrast to chemical and thermal processes that depend exponentially on activation energy. It is this relative insensitivity to the properties of the target material that gives sputtering the universality.

When the ion energy is less than the target atom's energy, the incident ion will be reflected with significant fraction of its initial energy. The fraction for 180^0 reflection becomes

$$f = \frac{(M_i - M_t)^2}{(M_i + M_t)} \qquad \text{Equation 2-2}$$

If M_i>M_t, reflection requires more than one collision and the reflection coefficient is low.

Since the ions have a high probability of being neutralized prior to impact, they are reflected as energetic neutrals which are therefore not influenced by the electric field over the target surface. The flux of reflected species contributes to substrate heating, particularly in devices operating at low pressures where the reflected neutralized ions may reach the substrates with little loss of kinetic energy by gas-phase collisions. Consequently, the reflected species bombard, and can become entrapped in, the growing film.

2.5.3 Sputtering Yield

The sputtering yield γ is simply defined as the ratio of the number of emitted to the number of bombarding particles.

$$\gamma = \frac{\text{No.of ejected particles}}{\text{No.of incident particles}} \qquad \text{Equation 2-3}$$

The yield depends on the target species and the nature, energy, and angle of incidence of the bombarding species. It is relatively insensitive to the target temperature. At sufficiently high temperatures, of course, the evaporation rate becomes of the order of, or larger than, the sputtering rate. The yield is also independent of whether or not the bombarding species is ionized. In fact, incident ions have a high probability of being neutralized by a field-emitted

electron prior to impact. Molecular bombarding species behave as if the atoms of the molecule arrived separately with the same velocity as the molecule and initiated their own sputtering events.

The sputtering yield tends to be greatest when the mass of the bombarding particle is of the same order of magnitude or larger than that of the target atoms. The use of inert-gas ions avoids chemical reactions at the target and substrate. Accordingly, Ar is often used because of its mass compatibility with materials of engineering interest and its low cost.

Sputtering yields are determined experimentally. Figure 2-5 shows yield versus ion-energy data for several materials under normal ion incidence. Additional data are given in Table 2-3. The dependence of the yield on the bombarding-ion energy exhibits a threshold of 20-40 eV, followed by a nearly linear region which may extend to several hundred eV. At higher energies, the yield verses ion-energy dependence becomes sub linear. The sputtering process is most efficient from the standpoint of energy consumption when the ion energies are within the linear range.

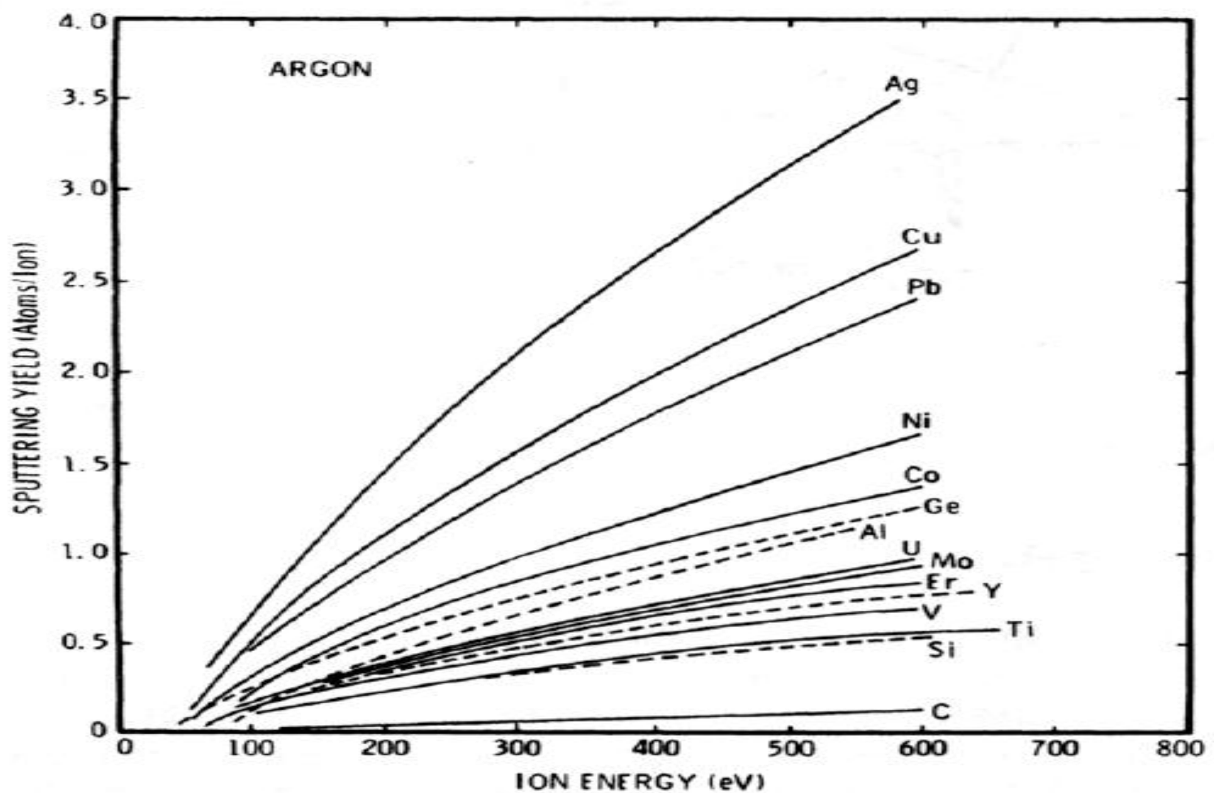

Figure 2-5: Variation of the sputtering yield of several materials as a function of Ar+ ion energy at normal angle of incidence [6].

Table 2- 3: Measured sputter rates for E = 500 eV argon ions at 1mA/cm^2 [6].

Target Material	Deposition Rate (Å / min)	Target Material	Deposition Rate (Å / min)
Be	159	Dy	1040
C	40	Er	881
Al	630	Hf	590
Si	310	Ta	380
Ti	336	W	340
V	337	Re	470
Cr	530	Os	440
Mn	874	Ir	540
Fe	429	Pt	792
Co	510	Au	1553
Ni	570	Pb	3073
Cu	818	Bi	8798
Ge	900	Th	740
Rb	4000	A12O3	129
Y	837	SiO2	400
Zr	570	CdS	2100
Nb	390	GaAs (110)	1500
Mo	421	GaP (111)	1400
Ru	580	GaSb (111)	1700
Rh	650	InSb	1300

2.5.4 Sputtering Configurations

The simplest form of sputtering is plasma based sputtering. In this type of configuration plasma is generated and positive ions are accelerated to the cathode (target material is at the cathode). Upon applying the low pressure environment, the positive ions reaching to the target surface due to the energy given by the potential drop between the surface and the point in the electric field at which the ion is formed. At higher pressures, the ions suffer physical collisions and charge exchange collisions so there is a spectrum of energies of the ions and neutrals bombarding the target surface.

Different power supply sources, such as DC or RF, are used to operate the sputtering process. These will be discussed in the following section.

2.5.4.1 DC-Plasma Sputtering

In Dc sputtering, target material is placed at the cathode while the substrate is placed on the anode which is often at ground potential. For cold cathode Dc diode sputtering, the top plasma-facing surface of the cathode is covered with a target material and the reverse side is water-cooled. The glow discharge can be generated by applying several kilowatts of dc voltage with series resistance of 1 to 10KΩ and kept the sputtering chamber in Ar gas at 0.1 Torr. The Ar ions generated in the plasma are accelerated towards the cathode and sputter the target resulting in the deposition of thin film on the substrates.

In the dc diode system, sputtered particles collide with gas molecules and then eventually diffuse to the substrate since the gas pressure is so high and the mean free path of the sputtered particles is less than the electrode spacing. The cold-cathode DC discharge can be sustained at argon gas pressures higher than about 10 microns. At these pressures, atoms sputtered from a cathode surface are rapidly thermalized by collisions in the gas phase. Sputtered deposition is not possible in that case, whenever pressure goes beyond 100 mTorr, then the sputtered material from the surface is scattered back to the electrode.

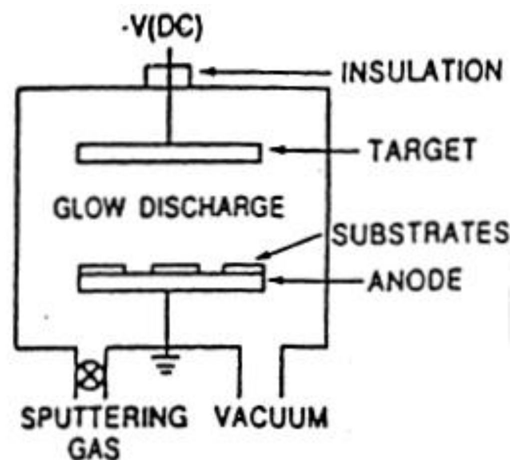

Figure 2-6: Dc diode sputtering system [5]

The cathode used in the Dc diode discharge must be an electrical conductor since an insulating surface will develop a surface charge that will prevent ion bombardment of the surface. If the target is initially a good electrical conductor but develops a non-conducting or poorly-conducting surface layer, due to reaction with gases in the plasma, surface charge buildup will cause arcing on the surface. This “poisoning” of the target surface can be due to

contaminant gases in the system or can develop during reactive sputter deposition from the deliberately introduced process gases.

Now for finding the deposition rate and the amount of sputtered particles, the amount of sputtered material deposited on a unit substrate area A is given by

$$A \cong k_1 A_0 / pd \qquad \text{Equation 2-4}$$

Where A is the density of the sputtered film, $k_1$is a constant, p is the discharge gas pressure and d is the electrode spacing.

The deposition rate is given by

$$R = \frac{A}{t} \qquad \text{Equation 2-5}$$

2.5.4.2 RF-Plasma Sputtering

Rf diode sputtering is used both for conducting and insulating materials. Since in the Dc plasma sputtering whenever insulating material is used, the sputtering glow discharge cannot be sustained because of the immediate build-up of a surface charge of positive ions on the front side of the insulator. To sustain the glow discharge with an insulator target, the dc voltage power supply is replaced by an rf power supply. This system is called an rf sputtering system.

Rf diode sputtering was first observed by Robertson and Clapp in 1933. They found that the glass surface of the discharge tube was sputtered during the rf discharge. In the 1960's, sputtering in the rf-discharge has been used for the deposition of dielectric thin films and a practical rf-sputtering system was developed. Rf diode sputtering system is shown in the Figure 2-7.

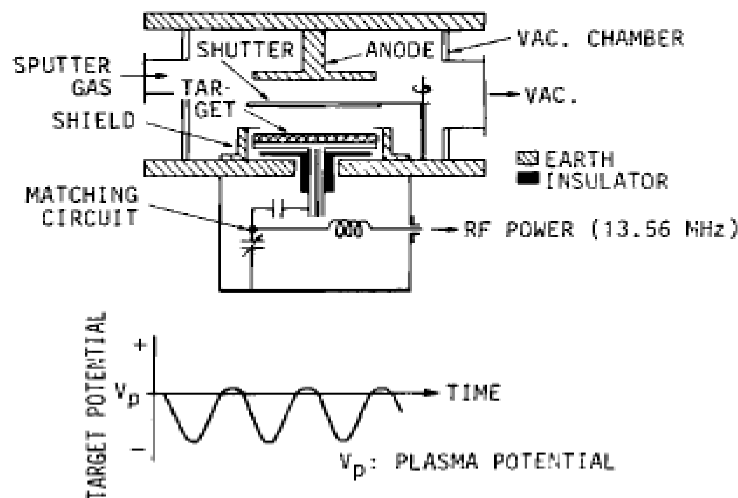

Figure 2-7: RF diode sputtering system [5].

Rf frequencies used for sputter deposition are in the range of 0.5–30 MHz with 13.56 MHz being a commercial frequency that is often used. Rf sputtering can be performed at low gas pressures (<1 mTorr) [7-8]. Rf potential is basically alternative positive negative potential with large peak to peak voltage. When rf potential is applied to the cathode, the glow discharge generates. During part of each half cycle, the potential is such that ions are accelerated to the surface with enough energy to cause sputtering while on alternate half-cycles, electrons reach the surface to prevent any charge buildup. The target surface is capactively coupled to the plasma, so it makes no difference whether the target surface used is insulative or conductive. The rate of the sputtering process is low compared to dc sputtering. The major drawback of the rf diode sputtering is that it is not working well when dielectric target material is used. Since most of the bombarding energy produces heat, this means that large thermal gradients can be generated that result in fracturing the target if high power levels are used.

2.5.5 Magnetron Sputtering

Magnetron-based sputter tools deposit thin films at relatively high deposition rates, with low substrate heating and over large deposition areas. The development of high performance magnetron sputtering sources modernized the sputtering process by greatly expanding the range of feasible applications. In a diode glow discharge arrangement, electron trajectories are only defined by the electrical field between the cathode and the anode. Hence, the electrons are accelerated over the cathode sheath, and move with high velocity toward the anode. To ensure that the electrons produce sufficient ions to sustain the discharge, the pressure must be quite high, i.e. of the order of a few Pa. To avoid the rapid loss of electrons from the discharge, classical approach can be applied in the form of a magnetic field. By applying a magnetic field during glow discharge sputter deposition, one can trap the electrons in the discharge longer and, hence, produce more ions for the same electron density. Restriction of these electrons to remain close to the target surface increases their probability of ionizing the working gas. This results in a more intense plasma discharge that can be sustained at a lower pressure. Since the ions are heavier than electrons, they are not affected by the confining magnetic field and may sputter much as in a diode type configuration.

The electron confinement is based on the Lorentz force given by the vector cross product of two field $\vec{E}$ and $\vec{B}$. Since $\vec{E}$is $\vec{B}$perpendicular to the target surface, application of a $\vec{B}$ field tangential to the surface gives the electron a component of velocity parallel to the target. Forcing the electrons in plasma, to move in a helical path, results in a great increase in

a probability that an electron will have a collision with a gas atom, leading to either exciting or ionizing the atom before being scattered out of the plasma region. This effect can be used to form very dense, low-impedance plasma. A single electron from the target can generate at least 10 electron-ion pairs in the volume of magnetized plasma.

Magnetron sputtering sources can be defined as diode devices in which magnetic fields are used in line with the cathode surface to form electron traps which are so configured that the $\vec{E} \times \vec{B}$electron drift currents form a closed loop path upon themselves. Magnetrons can be configured in a variety of forms. Examples include the planar magnetrons shown in Figure 2-8(a), the S-gun type shown in Figure 2-8(b), and the cylindrical type shown in Figure 2-9.

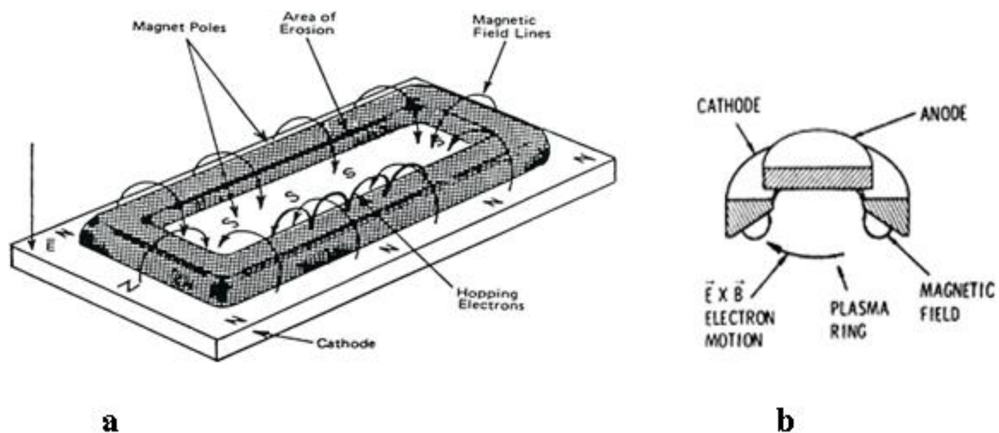

Figure 2-8: Magnetrons with magnetic end-confinement: (a) planar magnetron (b) gun type [5-8].

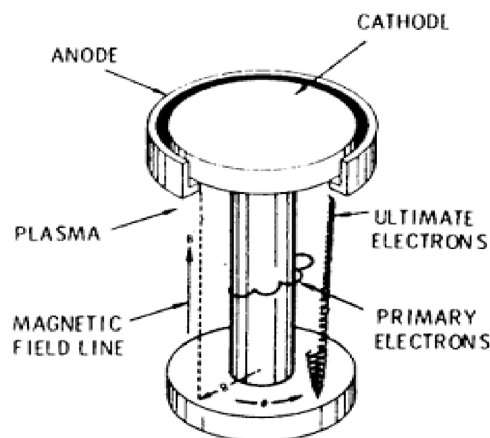

Figure 2-9: Cylindrical magnetron sputtering source with electrostatic end confinement [8].

2.5.5.1 The Planar Magnetron

Magnetrons make use of the fact that a magnetic field configured parallel to the target surface can constrain the motion of secondary electrons ejected by the bombarding ions, to a

close vicinity of the target surface. An array of permanent magnets is placed behind the sputtering source. The magnets are placed in such a way that one pole is positioned at the central axis of the target, and the second pole is placed in a ring around the outer edge of the target. A schematic of the magnetron is shown in Figure 2-10.

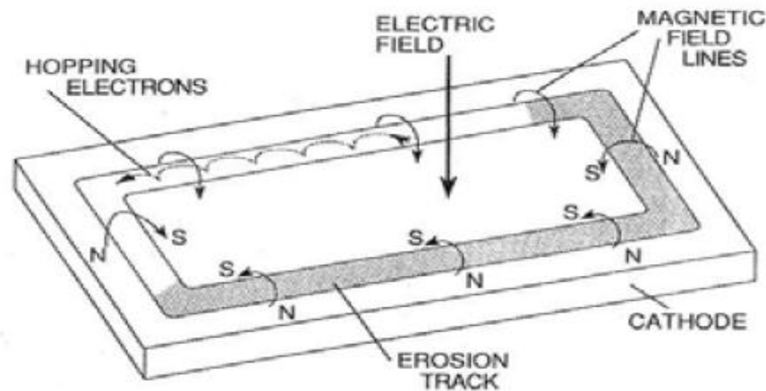

Figure 2-10: The principle of a magnetron [10].

The electrons which are emitted from the target surface due to ion impact are accelerated by the potential over the sheath. The trajectory of the electrons is greatly influenced by applying the magnetic field, which force them in cycloidal orbits. Thus bringing these electrons back to the cathode where they make a collision. The electron trajectory can be described by the Lorentz equation:

$$\vec{F} = q(\vec{E} + (\vec{V} \times \vec{B}) \qquad \text{Equation 2-6}$$

where q is the negative charge on the electron, E the electric field over the dark space, B the magnetic field, and v the velocity of the electron. Once the electron has left the cathode sheath, its trajectory is defined primarily by the magnetic field.

The Lorenz force on the electron is directly proportional to its velocity and the magnetic field strength, and is orthogonal to both their directions. The first component of the electron motion is the movement along the magnetic field lines. A second component is the gyration of the electrons around the magnetic field lines with the Larmor radius:

$$r_L = \frac{mv_\perp}{qB} \qquad \text{Equation 2-7}$$

in which $v_\perp$is the velocity of the electron perpendicular to the target.

Finally, the third component of the electron trajectory is the $\vec{E} \times \vec{B}$Hall drift. This drifting 'around' the post in a helical motion occur perpendicular to the electric and magnetic fields. This means electrons can move continuously in one direction around the target and are accelerated and decelerated close to the target surface.

The formation of the closed loop path for the $\vec{E} \times \vec{B}$ drifting secondary electrons is what defines a magnetron. The simplest geometrical design is circular planar magnetron. As the example of the trapping efficiency of the 15 cm cathode, it was shown that generally the electrons can be considered to go around the $\vec{E} \times \vec{B}$ loop from 3 to 8 times before they are lost to the walls of the system. The circular planar magnetron is the most widely used example. Since the overall requirement is simply that the $\vec{E} \times \vec{B}$ drift path form, there are many other geometrical perturbations. A common example is the rectangular planar magnetron shown in Figure 5.1. This geometry is similar to the circular planar one, but is simply stretched in one direction, forming an $\vec{E} \times \vec{B}$ drift path somewhat like a racetrack oval. Dimensionally, there is no real limit to the length of the rectangular cathode, and sources have been constructed several meters in length for the systems, where samples pass by the long sides of the cathode.

2.5.5.2 Magnetron Operation

Magnetrons can be operated in a number of ways depending on the application. In the simplest case, a direct current (DC) is applied to a single (conducting) target. Compound films can be grown in several ways. If the compound is conducting, a coating may be produced from a target of the same composition as the desired film. It is also possible to use multiple magnetrons of different target materials. Another alternative is to use a pure metal target in combination with a reactive gas. Reactions between the sputtered material and the reactive gas can now take place at the film surface and a compound film can be grown. In this way TiAlN can be reactively grown by using a single TiAl target, or by using separate Ti and Al targets, in a N2 environment. If the desired coating is not electrically conducting, DC sputtering from a compound target is not possible (for example Al2O3, which is a common coating material in industry). If a DC voltage is applied to such a target, the surface is charged up, and the sputtering process will immediately stop. This problem can be overcome in two ways; by using a metal target in a reactive environment or by the use of a quickly oscillating voltage. If one chooses the reactive alternative, one must keep a very good control over the partial pressure of the reactive gas. If too much gas is supplied to the discharge, the

target surface will be “poisoned”, and the sputtering stops, or gets very inefficient (low rate, or a lot of arcing). On the other hand, if one does not supply enough gas, the compound will not form with the right stoichiometry. The partial pressure must, therefore, be controlled so that it keeps the pressure at a level where the target is kept relatively “clean” by the sputtering, but there is enough gas to form the desired stoichiometry. This can be a quite complicated and unstable process. The other alternative is to use an alternating voltage of some kind (pulses or other type of oscillating voltage). The two most common ones are rf frequency sputtering (usually 13.56 MHz) or bipolar pulsed sputtering. In rf sputtering most materials can be used as cathode, but the deposition rate is usually very low. In bipolar pulsed sputtering, the voltage is reversed for a short time. This attracts some of the electrons from the plasma, and neutralizes the charge that has accumulated on the target surface. Since the electrons have so high mobility, it is usually only necessary to have a reversed bias supplied for 10–20 % of the time.

2.5.5.3 Balanced and Unbalanced Magnetron Sputtering

In the conventional balanced magnetrons the plasma is strongly confined to the target region. A region of dense plasma typically does not extend more than few cm from the target. Films grown on substrates positioned within this region will be subjected to strong ion bombardment which can strongly influence the structure and properties of the growing film. Substrates placed outside this region will lie in the area of low plasma density. Consequently, the ion substrate current is generally insufficient to modify the structure of the film. The energy of the bombarding ions can be increased by increasing the negative bias applied to the surface, however, this leads to defects in the film and increased film stress. To deposit dense films without introducing excessive stresses, a high flux of relatively low energy ions is generally preferred. These conditions are readily provided by unbalanced magnetrons, ionized physical vapor deposition (IPVD) techniques using secondary plasma to ionize the sputtered particles and recently by high power pulse magnetron sputtering.

In an unbalanced magnetron the outer ring of magnets is strengthened (or weakened) relative to the central pole. Schematic representation of the plasma confinement observed in conventional and unbalanced magnetrons is presented in Figure 2-11. In the case of unbalanced magnetron, not all the field lines are closed between the central and outer poles in the magnetron, but some are directed toward the substrate and some secondary electrons are able to follow these field line. Consequently, the plasma is no longer strongly confined to the

target region, but is allowed to flow out toward the substrate. Thus relatively high ion current can be extracted from the plasma without the need to externally bias the substrate.

By unbalanced magnetron, substrate ion current densities approximately an order of magnitude higher than for a conventional balanced magnetron can be routinely generated. Unlike other ion-plating processes, in unbalanced magnetrons the ion to neutral atom ratio at the substrate remains almost constant with increasing deposition rate, which is almost directly proportional to target current.

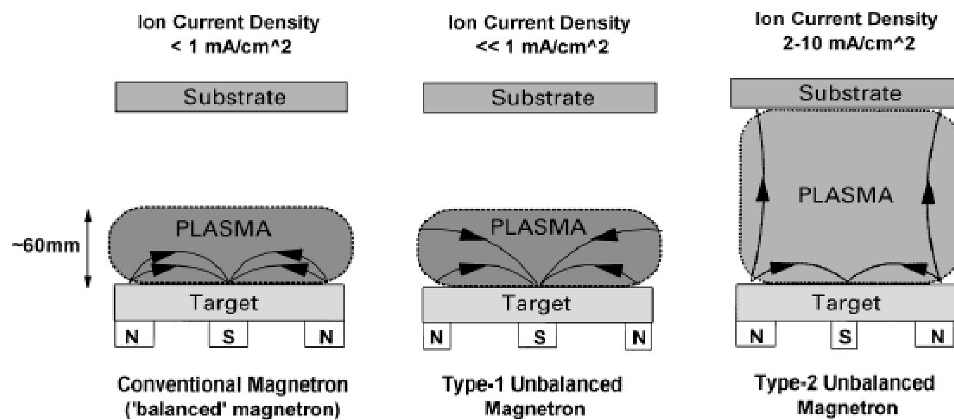

Figure 2-11: Schematic representation of the plasma confinement observed in conventional and unbalanced magnetrons [11].

2.5.6 Reactive Sputtering

Reactive sputtering is a method to deposit films which have a chemical composition different from that of the target, by adding a gas to react with the target material. The most common reactive gas is oxygen, usually mixed with argon to produce an oxide film.

An important phenomenon in reactive sputtering is the hysteresis behavior. A general hysteresis process is illustrated by the change of system pressure with varying flow rate of the reactive gas, say oxygen. Typically, the curve measured by increasing oxygen flow does not coincide with that measured by decreasing oxygen flow. There is a critical point along the increasing oxygen flow with two target modes. When the oxygen flow is smaller than the critical oxygen flow, the target is metallic, therefore metallic atoms are sputtered and a compound is formed on the substrate. So this is called the ‘metallic mode’. When the oxygen flow is bigger than the critical, the metallic target surface is ‘poisoned’ by formation of oxide on its surface; therefore it is called the ‘compound mode’. For metal targets, the target voltage after the critical point is dropped due to higher secondary-electron emission yields in the ‘compound mode’. The target voltage versus oxygen flow is used in our study to identify the critical oxygen flow. Figure 2-12 shows the target voltage for both increasing and

decreasing oxygen flow. For increasing oxygen flow, target voltage shows a sudden drop at a critical oxygen flow down to lower voltage value. For decreasing oxygen flow, target voltage keeps low as oxygen decreases pass the critical oxygen flow, and the voltage rises somewhere at oxygen flow which is lower than that critical value. Critical oxygen flow depends on operation conditions.

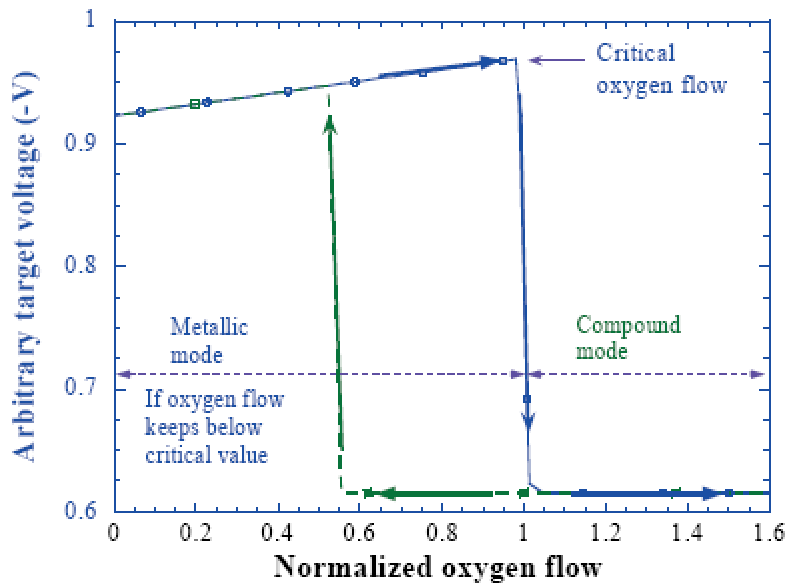

Figure 2-12: Scheme of target voltage versus oxygen flow rate showing hysteresis behavior. For increasing oxygen flow rate, target voltage shows sudden drop at critical oxygen flow [12].

2.6 PROPERTIES OF PVD THIN FILMS

Thin films formed by PVD techniques possess various properties required for different applications. In this section we will discuss how thin films formed microstructure evolution of PVD thin films and electrical and optical properties of PVD thin films.

2.6.1 Processes of Formation of Thin Film

The important Steps involved in the formation of a thin film are condensation, nucleation and growth on the substrate. Condensation can be defined as transformation of a substance from its vapor phase to the liquid or solid phase. Condensation can be initiated by the formation of small clusters or nuclei through combination of several incident atoms adsorbed on the substrate to form finally a coherent film, is termed as growth.

2.6.1.1 Condensation

Condensation can occur possibly if thermodynamic laws are obeyed. The partial vapor pressure of the substance in the gaseous phase should be equal to or greater than its vapor pressure in the condensed phase at the same temperature. If the substrate material is different from the vapor material, the impinging vapor atoms are first adsorbed on the surface of the substrate and condensation is initiated by the formation of small clusters of the adsorbed atoms. These small clusters then act as the initial centers of condensation. This Process can be defined in the following steps: when the impinging vapor atoms approach a few atomic diameters to the substrate surface. They would feel force due to the surface atoms of the substrate. Due to this force several interactions can occur. They are:

1. The impinging atoms may be reflected almost instantly retaining most of its kinetic energy,
2. The vapor atoms may also be physical adsorbed under the influence of Van der Waals force of the substrate atoms, which is called physi-sorption
3. There is also a possibility that chemical bond between a vapor atom and substrate atom may occur, in this case which is called chemi-sorption,
4. Impinging atom may form immediate association with other atom or atoms already adsorbed after finite stay time, or it may strike to the surface of the substrate and then migrate literally to join a cluster of adsorbed atoms.

The adsorption of incident vapor atom is possible only at that situation when there is thermal accommodation with the substrate atoms. If the kinetic energy of an incident atom is less than the energy of desorption, the thermal accommodation takes place by giving up its excess kinetic energy through lattice vibration of the substrate and the atom is adsorbed. Now under appropriate condition, whenever the rate of adsorption becomes greater than the rate of desorption, the small clusters (consisting of monomers) begin to enlarge, leading to stable nucleation and growth. The phenomenon of condensation has been studied by many researchers.

2.6.1.2 Nucleation and Growth

In the process of depositing thin film on a substrate the first stage is the formation of adsorbed monomers of one or more atoms which in the second phase, under the action force similar to surface tension, or capillarity combine to form small clusters. These clusters like the monomers are not stable and likely to be desorbed unless they attain a certain critical size

corresponding to a particular temperature of the substrate. On reaching a critical size, they continue to grow forming stable condensates.

Several theories are proposed to explain the formation of critical clusters leading to the growth of stable condensates. Out of all these, the two principal theories are the capillarity model and the atomistic model.

Capillarity model predicts that the free energy of a cluster passes through a maximum as it increases in size, and this maximum of free energy corresponds to the critical size of the cluster, which becomes stable above this critical size, but may re-evaporate below this critical size. This is similar to the process of formation of liquid droplets from vapors as explained by classical capillarity theory. Thus in order to condense a permanent deposit, aggregates of critical size or larger have to be created first. Critical nuclei can grow to super critical size either by direct incorporation of impinging atoms from the gaseous phase or by incorporation of the adsorbed monomers diffusing over the surface of the substrate. In the latter process, the rate at which the critical nuclei grow is given by the initial number of nuclei per unit area of the substrate and the rate at which the adsorbed monomers diffuse to join them. Capillarity model of the theories of nucleation enables one to evaluate free energy of formation of cluster of critical size and shows as to how the critical size and nucleation rate depend on the substrate temperature, impingement flux and the nature of the substrate.

The atomistic or small cluster model of the theories of nucleation is most identical with the capillarity model. In this case emphasis is given not on the free energy but on the dissociation energy of a critical cluster under specific condition of super saturation, and then the rate of nucleation corresponding to such a critical cluster is computed, leading to an expression involving parameters like number of monomers in the critical cluster, activation energy for desorption, activation energy for diffusion, substrate temperature, etc. The important prediction to be noted in this theory is that if the size of the critical nucleus changes by even one atom with super saturation, a discontinuity will occur in the nucleation rate versus temperature curve, and this may be verified experimentally.

By comparing the results of nucleation process derived from capillarity and small cluster models, Lewis, shows that the fundamental concepts underlying the two models are identical. The essential difference between them is that the small cluster model uses discrete arrangement of atoms whereas the capillarity model uses simple geometrical shapes of the clusters.

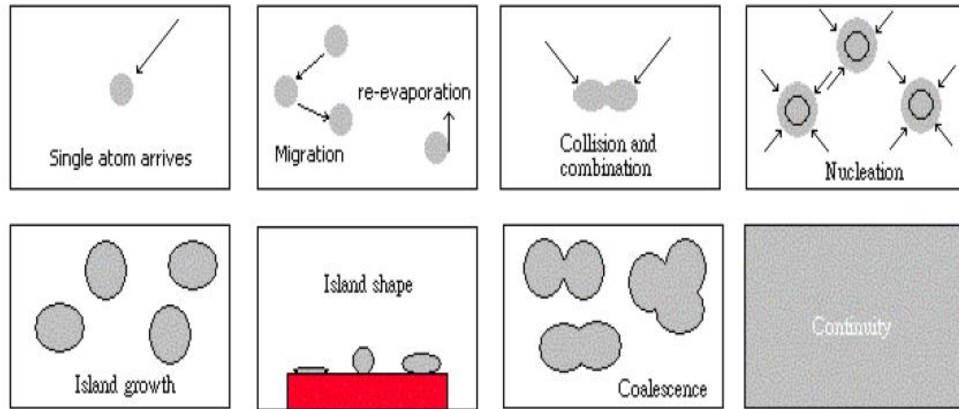

Figure 2-13: Thin film growth process [10].

2.6.2 Microstructure Evolution-Structure Zone Model (SZM)

As we have discussed earlier that thin films are formed by the process of nucleation and growth. The nucleation process depends upon interaction between the ad atoms and the substrate. When the nucleation process is going on the nuclei made on the substrate depends on the relative interfacial free energies between the film and the substrate γ_{fs}, the film and the vapor γ_{fv}, and the substrate and the vapor γ_{sv} [10]. The equation which shows the balancing of interfacial free energies at the interface is given by

$$\gamma_{sv} = \gamma_{fs} + \gamma_{fv}\cos\theta \qquad \text{Equation 2-8}$$

where θ is the contact angle. The phenomenon of the nuclie formation on the substrate is shown in the Figure 2-14.

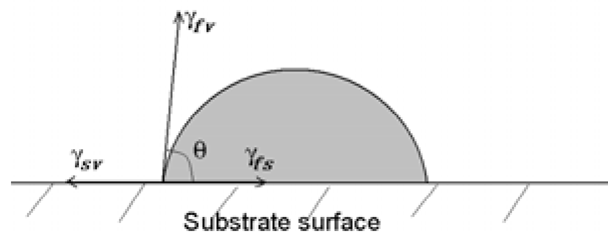

Figure 2-14: Schematic of a nucleus and the corresponding free energies [10].

Thin film growth occurs initially through three main stages [13]:

1. If $\gamma_{sv} \geq \gamma_{fs} + \gamma_{fv}$ and $\theta = 0$, it means the molecules or atoms in the growing film are bound more strongly to the substrate, than to each other. This type of growth is called layer by layer growth or 2-dimensional Frank-Van der Merwe (FM) growth mode.
2. If $\gamma_{sv} < \gamma_{fs} + \gamma_{fv}$ and $\theta > 0$, it means the molecules or atoms in the gwoing film are bound more strongly with each other, than to the substrate. This type of growth is called 3-dimensional Volmer Weber (VM) growth mode or island growth. The atoms

or molecules in the VM growth mode tend to aggregate with each other forming island with several monolayers.

3. This type of growth mode starts with a monolayer growth mode for a few monolayer and then shift into island growth. Actually this is a mixed type growth. This type of growth mode is called Stranski-Krastanov (SK) mode.

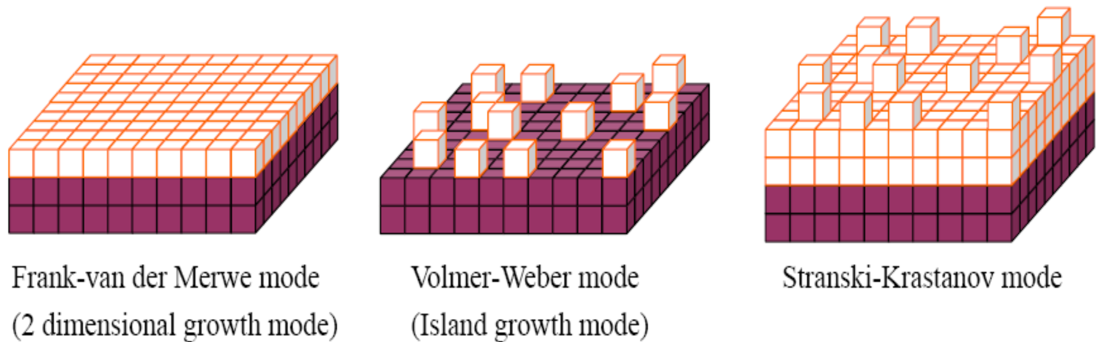

Figure 2-15: Different growth modes of thin film formation [10].

The thin film is influenced near the substrate by the substrate and/or interface material. Before the film grows through proper growth mode it takes an appreciable thickness. After the film growth occurs at the substrate, the film morphology can be described by a Structure Zone Model (SZM). The structural model was first proposed by Movchan and Demchishin for vacuum deposited coatings [14], Figure 2-17, and was subsequently modified by Thornton for sputtered deposited films as shown in Figure 2-18 [15].

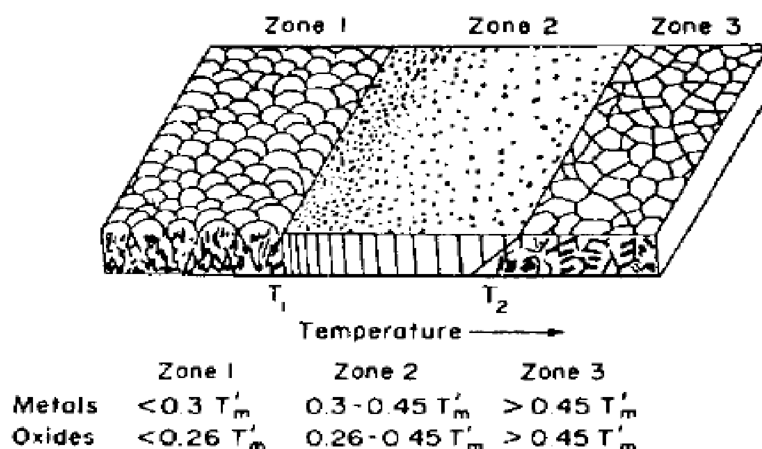

Figure 2-16: Structural zones in condensates [14].

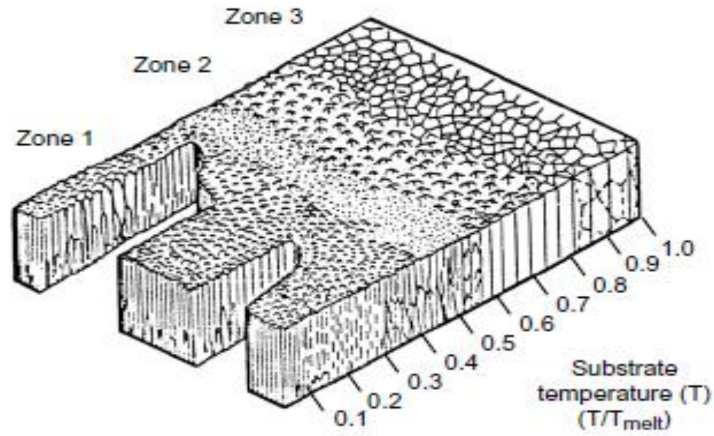

Figure 2-17: Structure Zone Model (SZM) of Vacuum Evaporated Condensates [14].

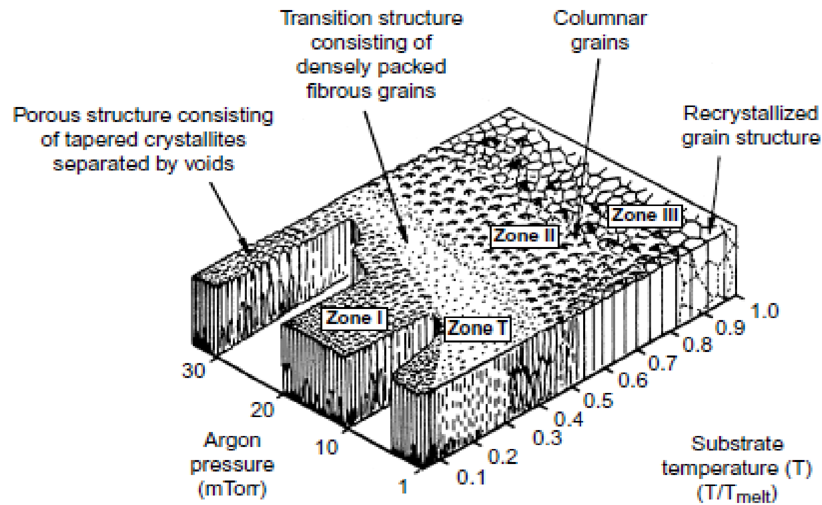

Figure 2-18: Structure Zone Model (SZM) of Sputter-deposited Materials [15].

During the process of deposition, the surface diffusion, the bulk diffusion, and the adsorption directly influence with the melting temperature of the deposit. Due to this reason it can result in four different film structures.

Zone I shows fine grain polycrystalline film forming amorphous structure. It is densely packed with crystallographic defects. At low T_s the surface mobility of the adatoms reduced i.e. at the absence of surface diffusion, the structure grows as tapered crystallites (columnar structure) from a limited number of nuclei. This type of zone contains longitudinal pores and high residual stress. Such type of zone is called Botryoidal (Figures 2-16 and 2-17).

Zone II shows a highly dense columnar structure with smother surfaces. This is due to the controlled surface diffusion growth. Due to surface energy anisotropy the columnar grains have highly faceted surfaces. Actually the grain size increases withT_s.

Zone III shows equiaxed grain morphology. The bulk diffusion allows recrystallization, grain growth and densification. This type of structure is obtained with highT_s.

Zone T is the transition zone between zones 1 and 2 [15], which shows tightly packed fibrous grains with weak grain boundaries. Actually this type of zone is observed when the gas pressure is decreased. A decrease in the gas pressure increases the energetic bombardments of the film.

As shown in the figure, for pure metals and alloys T_1 is the transition temperature between zone 1 and zone 2 and T_2 is the transition temperature between zone 2 and zone 3. According to Movchan and Demchishin's original model, $T_1$is 0.3 Tm for metals, and 0.22 to 0.26 Tm for oxides, whereas T_2 is 0.45 to 0.4 T_m (T_m is the melting point in°K).

2.6.3 Electrical Properties

2.6.3.1 Resistivity and Sheet Resistance

As we know that current flows in a material if there is a net flow of charges under the action of a potential gradient. Free electrons in the given material are accelerated due to the force $q\vec{E}$ upon applying the electric field. On the way free electrons collide with the other particles in the material (like phonons, impurity atoms, defects, etc.) so that's why free electrons move with average velocity known as drift velocity. As the movement of electrons is interrupted by their interaction with other particles, while they travel in the structure of the material, so this can be interpreted as electrical resistance of the material. Resistivity of a material is a property of the material in a given condition that measures the response of the material in terms of current flowing through it to an applied voltage. The electrical resistivity (δ) of a material is related to the resistance R and is given by given by:

$$R = \delta \frac{L}{A} \qquad \text{Equation 2-9}$$

where δ is the bulk resistivity in ohm-centimeters (Ω-cm), Lis the length of the conductor in cm, and Ais the cross-sectional area of the conductor in cm^2.

For a linear arrangement the sheet resistance is given by:

$$R_s = 4.532 \frac{V}{I} \qquad \text{Equation 2-10}$$

where Vis the measured voltage and Iis the injected current.

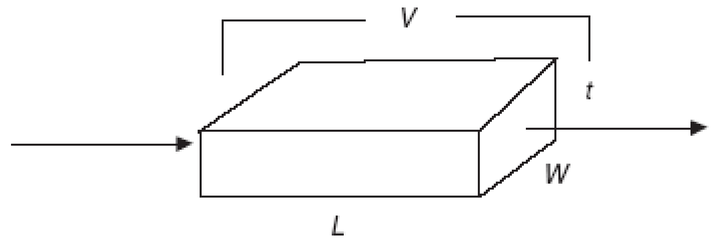

Figure 2-19: Resistance of a conductor by measuring the current I flowing for an applied voltage V. The sample has length L, width W and thickness t [9].

For a square of thin film of thickness (t) and side lengths of (L), the cross-sectional area becomes *L* x *t*and the resistance from side-to-side of any size square will be the same. This gives rise to the common thin film resistivity unit of ohms/square (Ω/sqr□) which is called the sheet resistivity (R_s). To obtain the resistivity of the film material in ohm-cm, the film thickness must be known. Resistivity or sheet resistance can measured with the 4-point probe method where the current is injected through the two outer probes and the voltage drop between two inner probes is measured [16]. The resistivity of deposited metals films is generally higher than that of the bulk form of the materials. Mercury can be used as a contacting material on the probe tip to avoid damaging pressure-sensitive surfaces.

Now we are going to find the expression to compute the resistivity when a four-point probe is used to measure the resistance. As shown in the figure the four probes are touched with the flat wafer, where the current I, enters through probe 1 and leaves it though probe 4. The voltage is measured between the probes 2 and 3. All the probes are placed equidistant from one another at a distance d.

The current density is given by

$$j = \frac{I}{2\pi R^2} \qquad \text{Equation 2-11}$$

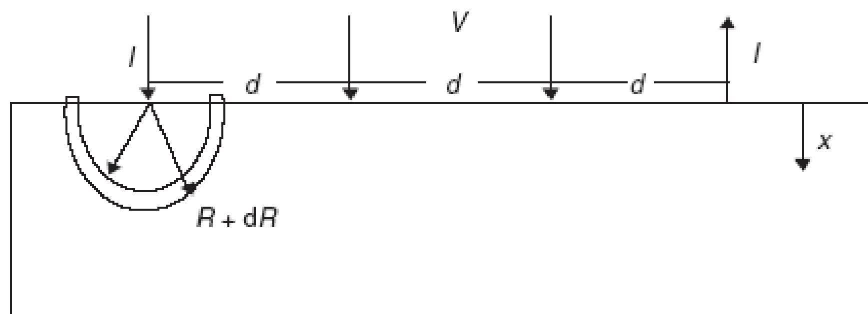

Figure 2-20: Measurement of resistance in a four-point probe [9].

The voltage V_{23}, measure between probe 2 and 3, is related to the current flowing by

$$V_{23} = \int_{d}^{2d} \frac{I}{2\pi R^2} \rho dR = \frac{I\rho}{2\pi d}$$

Hence,

$$\rho = \frac{2\pi d}{I} V_{23} \qquad \text{Equation 2-12}$$

2.6.3.2 Temperature Coefficient of Resistivity (TCR)

The temperature coefficient of resistance (TCR) of a material is the manner in which the resistance changes with temperature. On the basis of energy band theory, one can find the temperature dependence of resistivity for different materials. Metals and alloys have finite and nonzero density of energy states at the Fermi surface. There is also no gap in the energy band structure at the Fermi surface. So electrons can easily transfer from valence to the conduction band. Upon increasing the temperature there is very little probability to increase the number of carriers which participate in the conduction band. That’s why for metals TCR is positive i.e. increasing resistance with increasing temperature, while for dielectrics/semiconductors (tunnel type conductors), the TCR is negative i.e., the resistance goes down with temperature. To measure the TCR one only needs to combine a resistance measuring device with a temperature controlled environment.

The TCR of very thin metal films on electrically insulating substrates depends on the growth of the nuclei. Isolated nuclei result in a negative TCR due to the thermally activated tunneling conduction between nuclei. Connected nuclei, which form a continuous film, have a positive TCR as would be expected in a metal. Thus TCR measurements can be used to provide an indication of nucleation density and growth mode by determining the nature of the TCR as a function of the amount of material deposited. Often the film TCR is much less than that of the bulk material and may be of an opposite sign altogether. TCR measurements can give an indication of the perfection of the film material.

Changes of the electrical resistivity of a film having a columnar morphology, may be due to oxidation of the column surfaces. The combination of metallic conduction in the columns and the tunneling conduction through oxide layers on the column surfaces allows the formation of films that have a low, zero, or even negative thermal coefficient of resistivity (TCR) since the effects oppose each other.

2.6.4 Optical Properties

When light is incident on a semiconductor, the optical phenomena of absorption, reflection, and transmission are observed. From these optical effects, we obtain much of the

information. From absorption spectrum as a function of photon energy, a number of processes can be contributed to absorption. At high energies photons are absorbed by the transitions of electrons from filled valence band states to empty conduction band states.

Optical properties of films include the index of refraction, reflectance, and absorbance, each of which is a function of the wavelength, extinction (absorption) coefficient, optical scattering, index of refraction, and color.

The transmission coefficient T and the reflection coefficient R are the two important quantities generally measured. For normal incidence they are given by:

$$T = \frac{(1-R^2)\exp(-\frac{4\pi x}{\lambda})}{(1-R^2)\exp(-\frac{8\pi x}{\lambda})} \quad \text{Equation 2-13}$$

Where, $\boldsymbol{\lambda}$ is the wavelength of the sample. The equation can also be written as

$$T = \frac{(1-\bar{n})^2+k^2}{(1+\bar{n})^2+k^2} \quad \text{Equation 2-14}$$

Where, $\bar{n}$ is the refractive index, k the absorption constant, and x the thickness of the sample.

The absorption coefficient per unit length α is given by:

$$\alpha = \frac{4\pi k}{\lambda} \quad \text{Equation 2-15}$$

By analyzing the T–λ or R –λ data at normal incidence, or by making observations of R or T for different angles of incidence, both n and k can be obtained and related to transition energy between bands.

Reflective coatings reflect the incident radiation and what is not reflected is absorbed or transmitted. If there is spectral reflectance, the surface is a mirror. If there is scattering, the surface is a diffuse reflector like a white paint. For deposited metal films, the difference is generally the surface finish i.e. a smooth surface is necessary to make a good mirror.

Let us discuss the optical properties of ZnO thin films prepared by magnetron sputtering.

Transmittance and absorbance spectra of the produced ZnO thin films and glass slides are shown in Figures 2.20 and 2.21, respectively. By increasing O_2 ratio in total gas pressure (from 10% to 50%), transmission of the ZnO thin film increases from 69% to 80%.

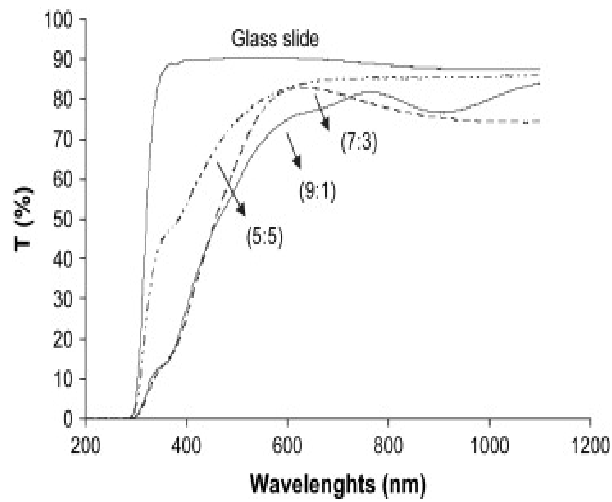

Figure 2-21: Transmittance spectra of produced ZnO thin films and glass Slides [17].

Figure 2-22 shows that absorbance at the wavelengths higher than 600 nm for all ZnO samples is very low. Differences in absorbance can be observed clearly at the wavelengths lower than 600 nm. These results shows that the produced ZnO materials could be used in photovoltaic applications due to the sharp increase of absorbance in strong absorption region corresponding to the wavelengths below 450 nm.

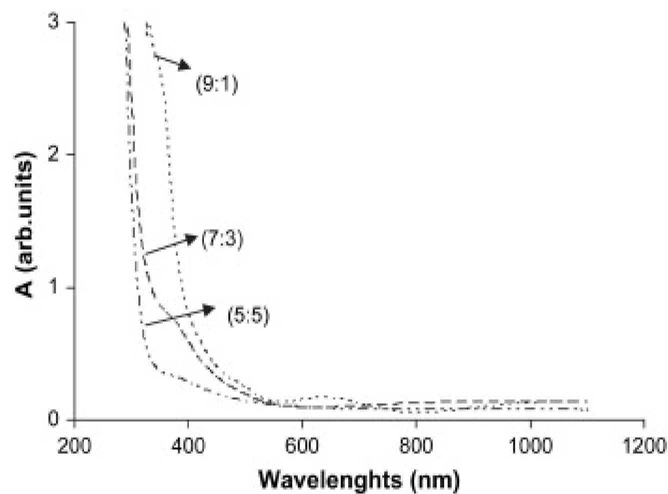

Figure 2-22: Absorbance spectra of produced ZnO thin films [17].

References

[1] J.O. Hirschfelder, C.F. Curtiss, R.B. Bird, Molecular Theory of Gases and Liquids, Wiley, New York 523 (1954).

[2] http://www.alacritas-consulting.com/sputter_deposition_for_thin_films.html

[3] Peter M. Martin, Physical Vapor Deposition, Columbia Basin Thin Film Solutions LLC Kennewick, (2009)

[4] http://www.thefullwiki.org/Sputter_deposition

[5] Wasa K. Hayakawa S., Handbook of Sputter deposition Technologies, Noyes Publications, New Jersey, (1992).

[6] Rointan F. Bunshah, Handbook of Deposition technologies, NOYES PUBLICATIONS, New Jersey (1994).

[7] Anderson, G.S., Mayer, W.N., Wehner, G.K., J.Appl.Phys., 33: 2291 (1962).

[8] Davidse, P.D., Maissel, L.I., J. Appl. Phys., 37: 754 (1966).

[9] M. D. Mattox, Handbook of Physical vapor deposition processing, Noyes Publications, New Jersey (1997).

[10] M. Ohring, Materials Science of Thin Films, Academic Press 2nd edition, San Diego (2002)

[11] P. J. Kelly, R. D. Arnell, Vacuum 56 159 (2000)

[12] http://www.freepatentsonline.com/6537428.html

[13] D. W. Pashley, Mat. Sci. Technol. 15 2(1999)

[14] B.A. Movchan, A.V. Demchishin, Study of the structure and properties of thick vacuum condensates of nickel, titanium, tungsten, aluminum oxide and zirconium oxide, Phys. Met. Metalogr. (Translation) 28 83 (1969)

[15] J.A. Thornton, High rate thick film growth, Ann. Rev. Mater. Sci. 7 239 (1977)

[16] Applied IMP Offers Ionized Sputtering, Solid State Technol., 39(11):54(1996)

[17] J. W. Hoon, K. Y. Chan, J. Krishnasam, T. Y. Tou, D. Knipp, Direct Current Magnetron Sputtered Deposited thin films, Applied Surface Science, 257 pp- 2508-2515 (2011)

CHAPTER NO 3

Thin Films for Solar Cells

3.1 INTRODUCTION

Smaller and faster is the technological imperative of our times and so there is a need for appropriate materials and processing techniques. Thin films play an important role in full filling this need. Besides, they have been used for device purposes over the past 45 years. Thin film is a two dimensional structure, i.e. it has a very high surface to volume ratio, and produced by the process of condensation of atoms, molecules or ions. They do the same function with the resultant bulk material and their material costs are smaller. Most of the electronic devices require consistent ohmic contacts for electrical signals to flow into and out of the device, and highly steady metal semiconductor resolving contacts as the active region. In both cases one must know how to fabricate consistent and proficient metal contacts which have high yield and stability. Thus, it is clear that knowledge of these devices can be used for the development of photovoltaic technology.

The demand for solar cells, although small compared with the overall energy supply (less than 0.1% of whole electricity consumption), has been developing promptly for the last several years. One reason for the growth in the thin film solar cell industry has been due to the polycrystalline Si unavailability for Si solar cells. Since the material used to fabricate Si solar cells needs to be about one hundred times thicker than the typical thin-film technologies to use the same amount of sunlight, small material usage is one of the most promising cost-effective schemes for thin film solar cell technology.

Thin film solar cells are considered as substitute to the commercially available, but too expensive crystalline silicon solar cells. The most successful thin film solar cells can be categorized as

1. Amorphous silicon (a-Si)
2. Cadmium telluride (CdTe)
3. Copper indium gallium di-selenide (CIGS)

The first two types of thin films solar cells are understood as an absorber/window structure: the absorber (CIGS or CdTe) is a p-type thin band-gap semiconductor of a few micrometer thicknesses. CIGS cells are usually slightly thinner (1- 3 µm) than CdTe cells (4-10 µm). The window layer is a very thin (< 0.1 µm) n-type wide band-gap semiconductor layer. Light of λ longer than the window cut-off wavelength K_c enters the cell through the window, and is absorbed in the absorber layer when its wavelength is smaller than the absorber cut-off wavelength (K_c ; 860 nm for CdTe and 950-1250 nm for CIGS). Figure 3-1 shows the basic strucures of thin films solar cells. In CIGS solar cells, both the window and the absorber can consist of a complex stack of layers: an outdated window structure is, e.g.,

n-CdS / i-ZnO / n $^{+}$-ZnO:Al; also the CIGSabsorber can consist of layers of different Cu (In, Ga) Se phases.

CdTe thin films solar cells typically have a more simple structure [1]. Figure 3- 1 illustrates that the electronic behavior of thin film solar cells is determined by various polycrystalline layers and the grain boundaries in between them.

Amorphous silicon thin films solar cells family are usually recognized as a pin structure, where an intrinsic layer of thickness well below 1 μm is inserted between two very thin, heavily doped extrinsic layers (Figure 3-1).

High efficiency thin film solar cells such as amorphous silicon (a-Si:H), copper indium-gallium di-selenide (CIGS), and CdTe are achieving ground in part due to their cost efficiency. Steady progress in energy conversion efficiency has been made both in the laboratory and industry scale for these thin film solar cells.

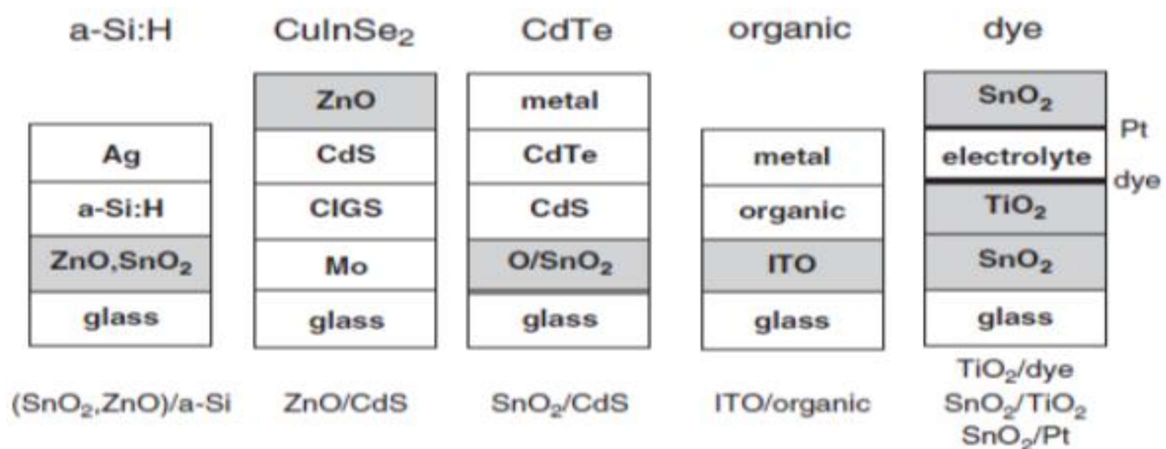

Figure 3-1: Schematic of different types of thin films cells [2-4].

3.2 CIGS THIN FILM SOLAR CELL TECHNOLOGY

3.2.1 Introduction

Copper indium gallium diselenide (CIGS) is a fascinating material for solar cell applications. CIGS is an alloy between copper indium diselenide (CIS) and copper gallium diselenide (CGS) and is described by the chemical formula $CuIn_{1-x}Ga_xSe_2$. The most important chalcopyrite compounds for photovoltaic applications are $CuInSe_2$, $CuInS_2$, and $CuGaSe_2$ with band gaps of 1.0, 1.5, and 1.7 eV, respectively. By changing the composition of Indium and Gallium in the alloy band structure can be varied between the two extreme values. This kind of choice is useful in solar cell applications both for a single layer solar cell as well as multilayer solar cells in altering the band gap of the P-type layer to best suit the

preferred application. Specifically, this range of energies is near the optimal energy for absorbing solar radiation with minimum losses. Since in the fabrication of CIGS thin film solar cell each layer is designed to absorb a different region of the incident solar spectrum. Therefore the choice to consider variation in the band gap energy is an advantage to construct more complicated, multilayer solar cells. CIGS also has a direct band gap which leads to the high absorption coefficient of this material. As a result of this high absorption coefficient and near optimal band gap energy CIGS is a leading material in the field of thin film solar cells.

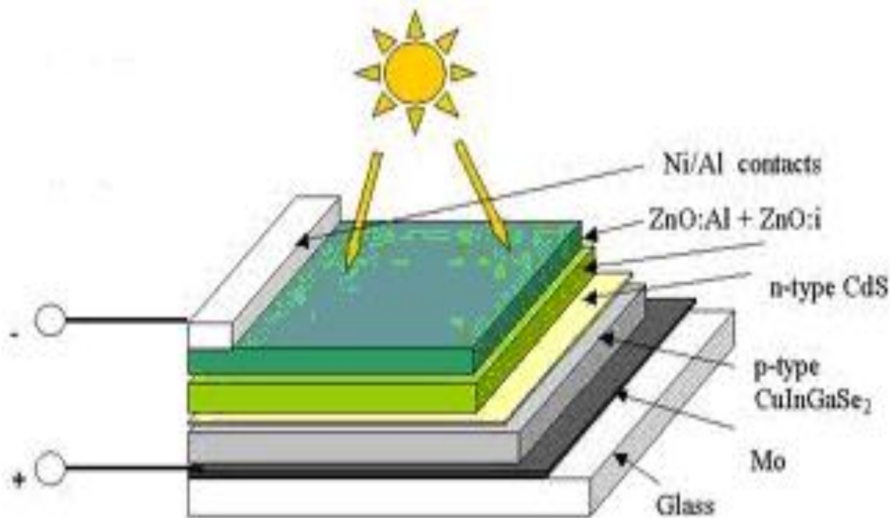

Figure 3-2: Structure of CIGS solar cell [5].

CIGS based solar cells have shown record efficiency (~20%) for thin film devices in testing [6]. This places CIGS solar cells at the forefront of the thin film solar cell industry. As the solar cell industry continues to expand there is great opportunity for CIGS based devices to become a significant technology in direct solar to electric conversion.

As a result of these factors, there is great potential for CIGS solar cells. There are several areas where additional research could greatly assist the use of CIGS as a practical solar cell device. The most important consideration with CIGS solar cells arises from their polycrystalline nature. The best solar cells from CIGS are not well ordered single crystals but rather a layer of multiple grains side by side, separated by grain boundaries forming a polycrystalline layer. In general, grain boundaries are detrimental to the performance of most modern microelectronic devices [7]. At grain boundaries, the uniform atomic structure of the grain is broken leading to variations in the potential energy of the atomic lattice at the boundaries. These variations disrupt the free flow of electrons and holes causing them to become trapped or scattered as well as providing defects in the lattice that assist in

recombination. For any semiconductor electronic device this interference in the free conduction of the charge carriers harms the overall performance of the device. Despite this general rule, polycrystalline CIGS solar cells perform better than single crystal cells. It is possible that the grain boundaries are where most of the defects in the lattice go leaving the grain interiors well-ordered and of high quality material. It is still not fully understood why these defects at the CIGS grain boundaries do not have the usual negative impact on performance as they do in most other materials. This lack of fundamental understanding of the operation of the solar cell device presents an important topic for research. If this could be understood it could be possible to engineer further improvements into the CIGS layer at the grain boundaries to achieve even better carrier conduction through the CIGS layer.

3.2.2 Device Structure

A typical Cu(In,Ga)Se_2 (CIGS) thin-film solar cell consists of the following layers shown in figure 3.4: a metallic (Mo) back contact; a p-CIGS absorber layer, the surface of which is usually intentionally made Cu-poor; an n-type (or intrinsic) buffer layer, usually CdS; an intrinsic ZnO layer, and an n-ZnO transparent front contact. Metallic Ni/Al contact grids complete the cell.

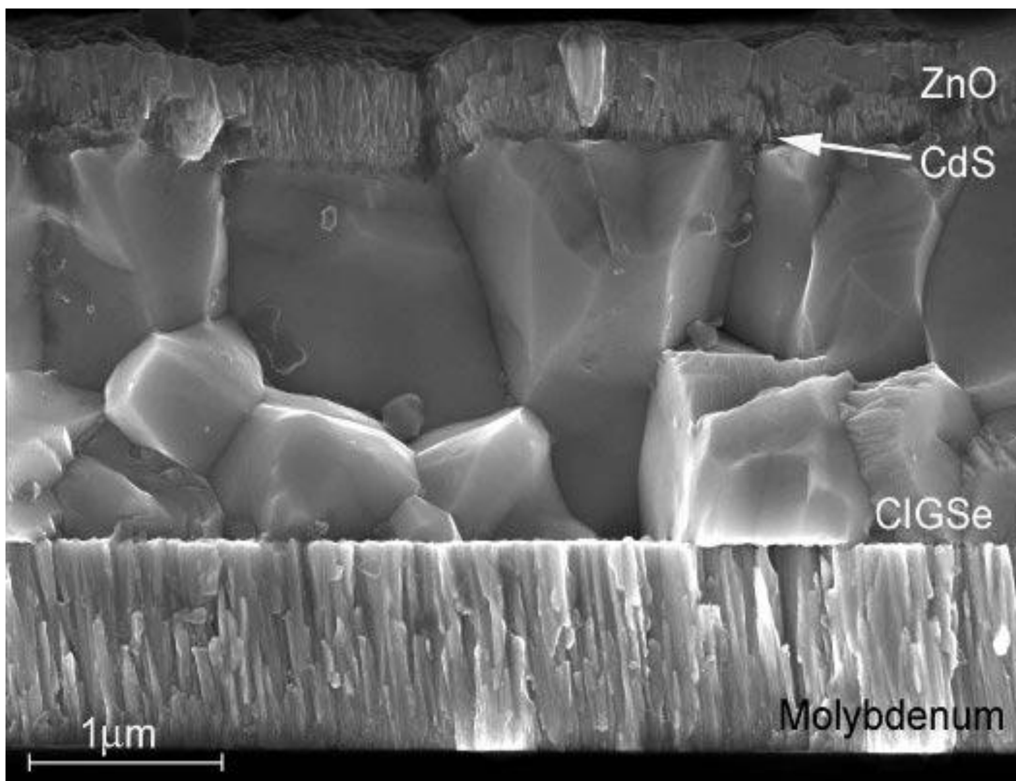

Figure 3-3: Scanning electron micrograph of the cross section of a typical chalcopyrite solar cell with Cu(In,Ga)Se_2 [8].

3.3 THIN FILMS FOR BACK CONTACT

3.3.1 Molybdenum Thin Films

Molybdenum (Mo) is the contact material commonly used in high efficiency solar cells. Thin films of Mo plays an important role in the formation of CIGS based thin film solar cells. Many papers have been written on the properties of Mo thin films [8]. The main properties of the Mo thin films which make it as proper back contact material for CIGS solar cells are

1. Inert during the deposition of the CIGS
2. To form an ohmic contact
3. Low recombination rate for minority carriers
4. Relative stability at the processing temperature
5. Low contact resistance to CIS and its alloys
6. Resistance to alloying with Cu and In

Mo has been reported by Scofield et al., [9] as a popular back contact material and dominant choice for the CIS and CIGS solar cells. Like other refractory metals deposited through physical vapor deposition techniques, Mo thin films were deposited through dc-magnetron sputtering [9]. Argon pressure and voltage were taken as process parameters. Scofield et al., [9] investigated that the lowest possible sheet resistance for back contact of the solar cell were obtained at the lowest Ar pressure. Films deposited at higher pressure passed the Adhesion test. Metals deposited through DC-magetron sputtering possess a correlation between the sputter gas pressure and the stress of the as-deposited film [9-10]. Thin films deposited with high pressure leads the film to be under tensile stress and thin films deposited with low Ar pressure leads the film to be under compressive stress.

Thin film Mo back contacts used in $Cu(In,Ga)Se_2$ solar cells play also a key role in enabling the diffusion of Na atoms from the underlying SLG substrate into the overlying $Cu(In,Ga)Se_2$ layer, where the Na is considered to improve the electronic properties of the $Cu(In,Ga)Se_2$ [10-11]. The Na out diffusion from the SLG into the $Cu(In,Ga)Se_2$ layer has been studied as a function of Mo deposition conditions [12]. These authors have demonstrated that the lower the sputtering pressure, the lower the concentration of Na in the $Cu(In,Ga)Se_2$ layer. Effectively, thin films of Mo prepared at low sputtering pressure formed densely packed grain structures, which prevent the migration of Na to the $Cu(In,Ga)Se_2$ layer, since the Na diffuses along the grain boundaries of the Mo film. A deposition pressure of ~5.0 mTorr was considered ideal in their system for the optimal Na concentration in the $Cu(In,Ga)Se_2$ layer.

When a thin film of Mo is deposited onto flexible substrates, it often creates cracks in the films [13]. To avoid the cracks in the film, it is a common practice to add oxygen during the fabrication of Mo thin films [14]. It is stated that, "optimum oxygen concentration is the minimum necessary to make the Mo film chemically inert against Se, where the heavy cracking of Mo back contact film during the deposition of Cu(In,Ga)Se_2 film has been found to be related to the reaction of Mo with Se in the deposition chamber. As such, minimizing the Se partial pressure in the system and localizing it to the deposition zone is considered as part of the solution to film cracking [14].

Jaegermann et al., [15] have reported that Mo produces a Schottky barrier p-CIGS. This is not in agreement with the fact that an ohmic back contact is necessary for obtaining high efficiency CIGS solar cells. It has been investigated that $MoSe_2$ interfacial layer is formed at the interface Cu(In, Ga)Se_2/Mo [16-17]. Basically $MoSe_2$ is a layered compound. The layer consists of Mo-layer embedded in between two layers of Se. The triple Se/Mo/Se layers are stuck together through weak van der waals forces, if there is present a covalent bond between Se/Mo/Se layers. T. Wada et al., [17] have investigated the CIGS/Mo interface and have suggested that CIGS/Mo hetro-contact without the $MoSe_2$ layer is not an ohmic, but schkotty type contact.

It is thus apparent from literature that the choices of deposition processes and parameters of the Mo thin film are essential for high efficiency Cu(In,Ga)Se_2 solar devices. Extensive research has been done on the deposition of Mo thin films by DC-sputtering [8-9-12]. However, as the potential portfolio applications of Cu(In,Ga)Se_2 expand, different film properties may be required to adapt to new necessities.

3.3.2 Features of Molybdenum Thin Films

Mo is a high melting point (2623 ^{0}C) refractory metal having bcc cubic crystal structure. Thin films of Mo are mainly deposited through PVD techniques such as magnetron sputtering and e-beam evaporation. As Mo thin films are used as a back contact materials (BC) in CIGS solar cells. Therefore the most obvious required properties for back contact material are low electrical sheet resistance, high conductivity and good adhesion to the substrate. The electrical properties and adherence to the substrate required for back contact material, stresses in thin films and Mo bilayer formation are reviewed in this section.

3.3.2.1 Electrical properties of Mo thin films

The electrical resistance of a material is a measure of its opposition to the passage of an electric current. Resistance of a material of uniform cross section is proportional to its length L, resistivity of the material ρ, and inversely proportional to its cross-sectional area A.

$$R = \rho \frac{L}{A} \qquad \text{Equation 3-1}$$

Sheet resistance can be defined as resistivity ρ per arbitrary square area d of the film.

$$R_s = \frac{\rho}{d} \qquad \text{Equation 3-2}$$

For a linear arrangement the sheet resistance is given by:

$$R_s = 4.532 \frac{V}{I} \qquad \text{Equation 3-3}$$

where Vis the measured voltage and Iis the injected current.

Mo thin films prepared through Dc-plasma magnetron sputtering shows that the resistivity found to decrease by increasing either the deposition power or the deposition time as shown in Figure 3-4(a). From the figure, it can be seen that the deposition time is less effective as the deposition power increases. This can be explained by the fact that the high deposition power enhances the quick growth of a relatively thick film. Since the increase of the film thickness leads to the decrease of the resistivity of the Mo films [18], the effect of the deposition time is reduced as the deposition power increases. Figure 3-4(b) shows that the resistivity decreases also by increasing the substrate temperature.

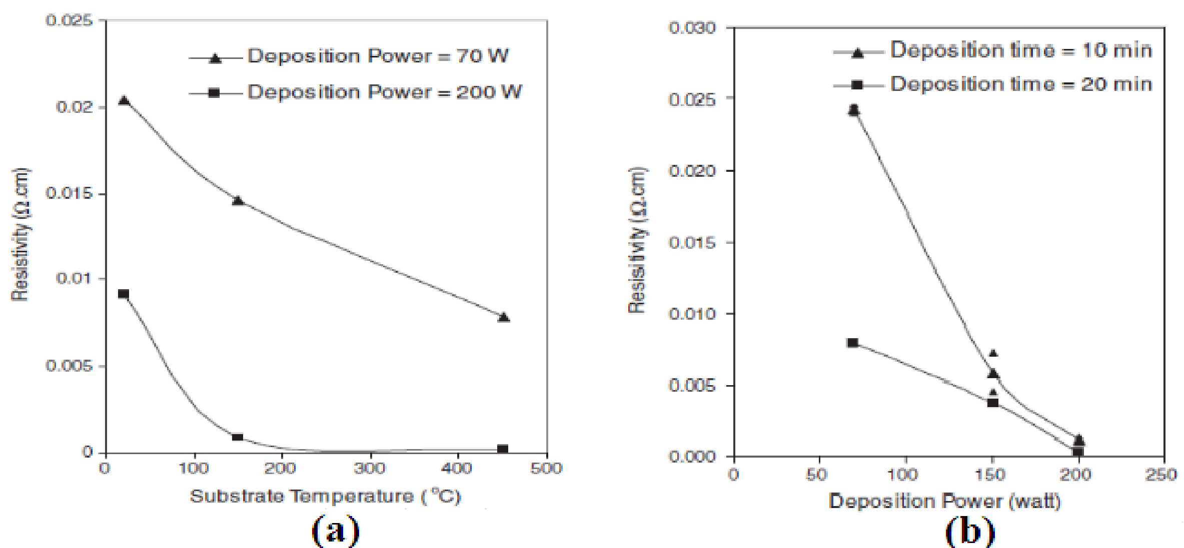

Figure 3-4: (a) Resistivity versus deposition power at different deposition times for films deposited on substrates at temperature of 450 ^{0}C. (b) Resistivity versus substrate temperature at different deposition powers for thin films prepared with deposition time of 20 min [18].

3.3.2.2 Stresses in Molybdenum Thin Films

Mo is a high melting point refractory metal, it is difficult to deposit this film without some residual stresses. Thin films of Mo mainly deposit through magnetron sputtering and e-beam evaporation. Among them typically used technique to deposit refractory metals is magnetron sputtering. A connection is observed between the sputter gas pressure and the stress of the as-deposited film. Films deposited with low Ar pressure are generally found to be under compressive stress, while those deposited with high Ar pressures are found to be under tensile stress. Gross stress may be determined by visual inspection in that highly compressed films tend to buckle up, frequently in zigzag patterns, whereas films under extreme tensile stress develop a system of stress lines that look like scratches [19]. Most of the Mo thin films shows mono-crystalline nature with crystallites found to have an orientation along (110) direction. The variation of the average lattice spacing; i.e., the slight shift of the (110) peak position, in the direction normal to the plane of the films, gives the strain in the films, which is either compressive or tensile. The strain in the films is calculated using the following formula:

$$\text{Strain}\ (\%) = \frac{\Delta a}{a} \times 100 \qquad \text{Equation 3-4}$$

where a is the lattice constant (for reference, a_{Mo}= 0.31469 nm), and the main parameter to determine whether the strain is tensile or compressive.

The origins of the strain profiles in the sputtered Mo films may be related to several factors, including voids, oxygen, or argon impurities, and crystallographic flaws [19]. The high strain in the films can cause adhesion problems and compromise long term reliability.

X-ray techniques for measuring the strain state of crystalline materials are well established. One approach involves evaluation of strain through measurements of inter-planar spacing as a function of sin θ is particularly well-suited for determining the strain state of metal films. For a continuous, non-passivated film the principal stresses that lie in the plane of the film are equal. In the direction perpendicular to the plane of the film, U_s = 0. The unstrained lattice parameter (d,) for a film can be found at a fixed value of $\sin^2\theta$, which is a function of the particular material and microstructure.

Figure3-5 shows the intrinsic stress value of the Mo films as a function of the working gas pressure. Films deposited at low pressures exhibited compressive stresses while those deposited at higher pressures exhibited tensile stresses. The stress in the films showed a transition from compressive to tensile with increasing working pressure.

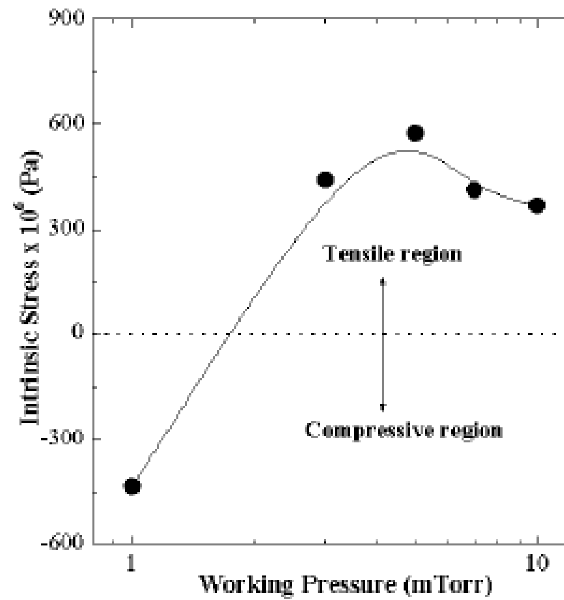

Figure 3-5: Variation of the intrinsic stress of Mo-sputtered films with the working gas pressure [20].

3.3.2.3 Adherence of Molybdenum Thin Films with the Substrate

Molybdenum thin films sputtered at different parameters shows dissimilar adhesion with the substrate. It is observed that Mo thin films sputtered at high Ar pressure shows good adhesion to the soda-lime glass substrates. While films sputtered at low Ar pressure delaminates from the substrate surface. Table 3-1 shows adhesion of film is related to Ar pressure and residual stresses in the film.

Table 3- 1: Summary of the adhesion tape test as function of Ar pressure and GIRXD in-plane stress parallel to (σ_{11}) and normal to (σ_{22}) cathode axis [9].

Ar Pressure (mTorr)	Adhesion Tape Test	Stress	
		σ_{11}(MPa)	σ_{22}(MPa)
0.2	Fail	-316	-505
0.5	Fail	61	-231
1.0	Fail	577	370
2.0	Pass	1141	1028
5.0	Pass	364	474
10.0	Pass	-7	22
20.0	Pass	-160	-167

In CIGS and CdTe based thin films solar cells 1st Mo layer is deposited on substrates because it promotes adhesion by reducing stress as the tensile layer before the compressive layer of Mo, and helps to smooth the rough surface of the substrate. A smooth substrate surface is required for two reasons [21]. First abrupt changes in the surface topography such as spikes or cavities may lead to shunts between the front and back contact, and degrade adhesion of the solar to the foil substrate. Second, the deposition of impurity diffusion barriers or buffer layers may be easier and more successful on a smooth substrate.

3.3.2.4 Molybdenum Bilayer Process

The basic requirement for CIGS based thin film solar cell is minimum sheet resistance as possible for Mo back contact layer. Literature review, results shows that films sputtered at high Ar pressure shows good adhesion to the substrate but having high sheet resistance while film sputtered at low Ar pressure shows delamination and low sheet resistance [9]. So Mo films sputtered at a single pressure do not simultaneously possess low resistivity and good adhesion, both of which are desirable characteristics for fabricating back contact metalized layers for solar cells. In order to circumvent this problem, an original two-pressure deposition scheme has been designed in which first a thin layer of "high pressure" Mo is sputter to serve as an adhesion layer, followed by the deposition of "low-pressure" Mo to achieve low sheet resistance.

3.3.2 Other Materials Used as Back Contact

Mo is used as an ideal back contact material, since from the origin of CIGS solar cells. But it contains some disadvantages which may be circumventing in order to make it not an ideal back contact. Corrosion of molybdenum [22] is one of the few known issues and has been reported to contribute to module degradation in accelerated lifetime testing. It is feasible that the stability could be improved by using molybdenum based alloys instead of pure molybdenum. Another disadvantage of molybdenum is its poor optical reflection which may become relevant in view of efforts to reduce the absorber thickness.

K.Orgassa [8] et al. investigated W, Mo, Ta, Nb, Cr, V, Ti and Mn as possible back contact material for CIGS solar cells. All the films were deposited by electron beam evaporation on soda lime glass. Subsequently CIGS layer was deposited by co-evaporation, CdS by CBD and ZnO by RF sputtering. They have concluded that Ti, V, Cr and Mn tend to react with Selenium during absorber growth thus affecting the absorber growth. Devices with Ta and Nb back contact showed good performance only with ordered band gap absorber.

Devices with a tungsten back contact showed comparable performance as devices with a Mo back contact, with and without band gap rating. The authors have also established a relation to calculate the current density loss due to the back contact. Tungsten seems to yield a good ohmic contact but its optical properties in this respect are poor. Tantalum and niobium have slightly higher reflections and initial studies [8] indicate that they may be feasible in terms of contact performance. Transparent conductive oxide coated metal contacts may be another solution to attain stability, and good electrical as well as optical performance for thin cells.

References

[1] X. Wu, J. Keane, R. Dhere, C. DeHart, A. Duda, T. Gessert, S. Asher, D. Levi, P. Seldon, in: B. McNelis, W. Palz, H.A. Ossenbrink (Eds.), Proc 17th Europ. Photovolt. Solar Energy Conf., WIP, Munchen, Germany and ETA, Florence, Italy, p. 995, (2001)

[2] B. Rech, H. Wagner,Amorphous and microcrystalline silicon solar cells prepared at high deposition rates using RF (13.56 MHz) plasma excitation frequencies, Appl. Phys. A 69, 155 (1999)

[3] K. Ramanathan, M.A. Contreras, C.L. Perkins, S. Asher, F.S. Hasoon,J. Keane, D. Young, M. Romero, W. Metzger, R. Noufi, J. Ward, A. Duda,Progr. Photovolt.: Res. Appl. 11, 225 (2003)

[4] R. Klenk, J. Klaer, R. Scheer, M.C. Lux-Steiner, I. Luck, N. Meyer, U. R¨uhle,Thin Solid Films 480–481, 509 (2005).

[5] http://www.solarnavigator.net/automotive_directory/honda.htm

[6] K. Ramanathan, M. A. Contreras, C. L. Perkins, S. Asher, F. S. Hasoon, J. Keane, D. Young, M. Romero, W. Metzger, R. Noufi, J. Ward, and A. Duda, Prog. Photovolt: Res. Appl. 11, 225-230 (2003).

[7] Möller, J. Hans,Semiconductors for Solar Cells (Artech House, Boston Massachusetts) (1993)

[8] K. Orgass, H. W Schock, J. H. Werner, "Alternative back contact materials for thin film Cu(In,Ga)Se2 solar cells." Thin Solid Films 431–432,387 (2003).

[9] J. H. Scofield, A, Duda, D. Albin, B. L. Ballard, P. K. Predecki, "Sputtered molybdenum bilayer back contact for copper indium diselenide based polycrystalline thin–film solar cells." Thin Solid Films 260, 26 (1995)

[10] J. H. Scofield, S. Asher, D. Albin, J. Tuttle, M. Contreras, D. Niles, R. Reedy, A. Tennant, R. Noufi, "Sodium diffusion, selenization, and micostructural effects associated with various molybdenum back contact layers for CIS–based solar cells." In: Proc. of the 24th IEEE Photovoltaic Specialists Conference pp.164 (1994)

[11] A. Rockett, "The effect of Na in polycrystalline and epitaxial single–crystal $CuIn_{1-x}GaxSe_2$." Thin Solid Films 480–481, 2 (2005)

[12] H. A. Al-Thani, F. S. Hasoon, M. Yang, S. Asher, J. L.Alleman, M. M. Al-Jassim, D. L. Williamson, "The effect of Mo back contact on Na out diffusion and device performance of Mo/Cu(In,Ga)Se2/CdS/ZnO solar cells." In: Proc. of the 29th IEEE Photovoltaic Specialist Conference pp. 720 (2002)
[13] F. Kessler, K. Herz, M. Powalla, M. Hartmann, M. Schmidt, A. Jasenek, H. W. Schock, "Flexible and monolithically integrated CIGS–modules." Mat. Res. Soc.Symp. Proc. 668, H3.6.1-3.6.6 (2001)
[14] E. Eser, S. Fields, G. Hanket, R. W. Birkmire, J. Doody, "Critical issues in vapor deposition of Cu(In,Ga)Se2 on polymer web: source spitting and back contact cracking." In: Proc. of the 31st IEEE Photovoltaic Specialist Conferencepp. 515 (2005)
[15] W. Jaegaerrmann, T. Loher and C. Pettenkofer Cryst. Res. Technol.31p. 273 (1996)
[16] S. Nishiwaki, N. Kohara, T. Negami, T. Wada, Jpn. J. Appl.Phys. 37 71 (1998).
[17] T. Wada, W. Kohard, S. Nishiwaki, T. Negami, Thin SolidFilms 387 118 (2001).
[18] A. E. Hady, B. Kashyout, H. M.A. Soliman, H. A. Gabal, P. A. Ibrahim, M. Fathy, Preparation and characterization of DC sputtered molybdenum thin films, Alexandria Engineering Journal 50, 57–63 (2011)
[19] S. G. Malhotra, Z. U. Rek, S. M. Yalisove, J. C. Bilello, "Strain gradients and normal stresses in textured Mo thin films." J. Vac. Sci. Technol. A 15, 345 (1997)
[20] K. H. Yoon, S. K.Kim, R. B. V. Chalapathy, J. H. Yun, J. C. Lee, J. Song, B. Tae Ahn, Characterization of a Molybdenum Electrode Deposited by Sputtering and Its Effect on $Cu(In,Ga)Se_2$ Solar Cells, Journal of the Korean Physical Society, Vol. 45, No. 4, 1114-1118 (2004)
[21] F. Kessler, D. Rudmann, "Technological aspects of flexible CIGS solar cells and modules", Solar Energy Materials & Solar Cells, 77, 685-695 (2004)
[22] J.Wennerberg, J.Kessler,M. Bodeg°ard, L. Stolt, Damp heat testing of high performance CIGS thin film solar cells, Proc. 2nd World Conf. Photovoltaic Solar Energy Conversion, Vienna, Austria,6–10 July 1998, J. Schmid, H. A. Ossenbrink, P. Helm, H. Ehmann, E. D. Dunlop (Eds.), JointResearch Center ISPRA 1161(1998)

CHAPTER NO 4

The Experiment

Preparation of Molybdenum thin films using DC-magnetron Sputtering

4.1 EXPERIMENTAL PROCEDURE

4.1.1 Substrate Preparation

Soda lime glass slides (Cat. No. 7105) were used as substrates for the deposition of molybdenum thin films through DC-magnetron sputtering. The SLG substrates were cut down to the size of 1cm×1cm×1mm. Substrates were cleaned using methanol, soap, chromic acid and distilled water. Initially the substrates were cleaned using methanol in an ultrasonic bath for 20 minutes. After scrubbing with soap, the substrates were dipped in chromic acid for 10 minutes. Finally the substrates were washed with distilled water using an ultrasonic bath for 30 minutes in order to remove impurities and contaminants from the surface of the substrate. After cleaning the substrate were dried.

4.1.2 DC-Magnetron Sputtering

Molybdenum thin films were prepared on 1cm×1cm×1mm SLG substrates by means of a DC-magnetron sputtering system ([*]Alliance Concept DP650). Mo was used as a target material. Substrates were subsequently introduced into the chamber. Before deposition of the thin film, target was pre-sputtered in an Argon atmosphere for about 15 minutes, so that any oxide layer remains on the surface of the target can be removed. For this purpose the shutter remains closed.

The procedure for depositing all the films was as under

1. The chamber was evacuated to a base pressure of 7.49×10^{-6}mbarr.
2. Pure Argon (99.99%) flow was introduced into the chamber. The flow rate of Argon was varied from 2 to 18sccm and the working gas pressure was varied from 0.002 to 0.0123mbarr.
3. The DC power supply was then turned on. The DC power was varied from 100 to 200W.

A series of eight Mo thin films were prepared by changing a specific parameter. The parameters include deposition power, Ar pressure and substrate temperature.

The experimental details are summarized in Table 4-1.

Table 4- 1: Summary of the deposition parameters for the preparation of Mo thin films

ID	Power (W)	Pressure (mbar)	Flow Rate (sccm)	Substrate Temp. (^{0}C)	Thickness (nm)	Time (min)	Rate (nm/s)
1	100	0.0123	18	RT	1000	14	1.19
2	100	0.0123	18	400	1000	14	1.19
3	200	0.0123	18	RT	1000	8	2.084
4	200	0.0123	18	400	977	7.49	2.084
5	100	0.002	2	RT	1000	15	1.11
6	100	0.002	2	400	1000	15	1.11
7	200	0.002	2	RT	1000	8	2.084
8	200	0.002	2	400	925	7.4	2.084

Different sets of thin films were prepared by changing a specific parameter and keeping the other parameter constant. The physical, electrical and structural properties of thin films were studied as a function of Ar pressure, deposition power and substrate temperature. The effect of each deposition parameter on the properties of deposited film can be summarized as

1. Effect of Ar pressure on the properties of deposited film
2. Effect of deposition power on the properties of deposited film
3. Effect of substrate temperature on the properties of deposited film

**** RF-Magnetron Sputtering System***

The system used has the following specs:

- Make & Model: Alliance Concept DP650
- Power Supplies: DC, RF, bias RF / DC
- Equipment is designed for any kind of application
- No of Targets: 6
- Maintain substrate temperature up to 400^{0}C.
- Limit vacuum in the 10^{-8} mbar range.

Figure 4-1: Alliance Concept DP650 RF-magnetron Sputtering System [1].

4.2 CHARACTERIZATION TECHNIQUES

The physical, electrical and structural properties of Mo sputtered thin films were characterized. Details of the characterization tools are given in the following sections.

4.2.1 Scanning Electron Microscope (SEM)

Scanning electron microscopy is a widely used technique for characterization of materials. SEM stands for Scanning electron microscopy and its name suggest that it uses electrons instead of light to take an image of the sample. In operational mode electrons are generated thermionic ally from a metal filament and accelerated to reach an approximate value of 25keV. SEM consists of electrical and magnetic optics. They are used to focus electrons beam to a spot on the sample surface. A schematic of SEM is shown in the Figure 4-2.

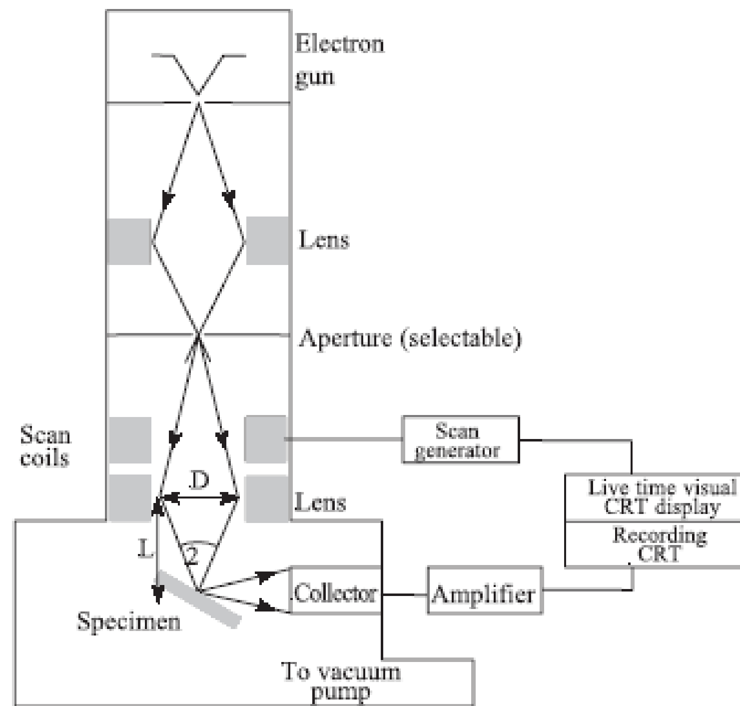

Figure 4-2: Schematic diagram of scanning electron microscopy [2].

SEM must be carried out at low pressure in the order of 10^{-6}torr. The sample needed for SEM analysis must be conductive. In case of insulating material, diamond will be coated on the sample using glow discharge sputtering. The electron beam is scanned or rastered across the sample surface through magnetic scan coils. The secondary electrons reflected from the sample surface are collected and amplified. Two dimensional micrograph of the sample from signal intensity obtained is created.

The surface morphology and cross-sectional study of Mo thin films were examined using Scanning Electron Microscope SEM (JEOL; JSM 6490LA) with operating voltage of 15-20kV, spot size of 30-50 and working distance of 10.

4.2.2 Atomic Force Microscope (AFM)

Atomic force microscopy is a very powerful microscopy technique, used for taking topographical images of surfaces. It is consists of a cantilever with a sharp tip connected at its ends. In the imaging mode, the sharp tip is rastered or scanned over the surface and a surface topographical image is obtained. The force between the surface and the tip leads to deflection of the cantilever according to Hook’s law. The deflection of cantilever is measured by reflecting a collimator laser beam on the top surface of the cantilever and taking image of the light spot on a two or four quadrant diode detector. The schematic of the AFM is shown in the Figure 4-3.

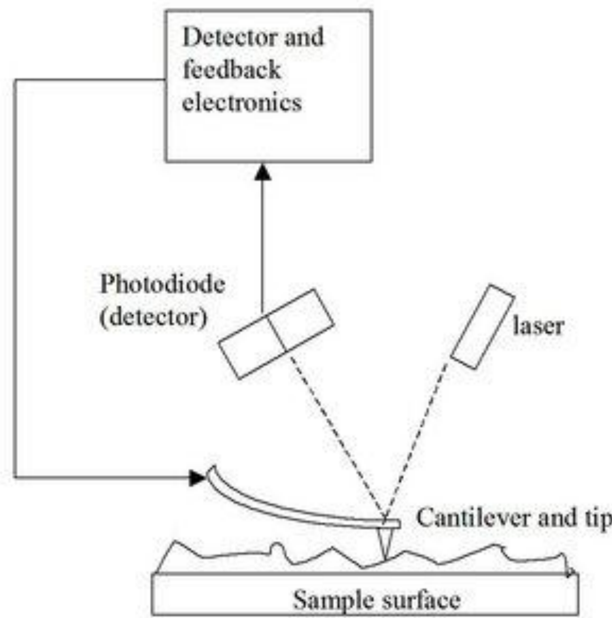

Figure 4-3: Schematic diagram of AFM [3].

AFM can operate in three modes such as contact mode, non-contact mode and tapping mode. In operational mode the tip of AFM is scanned across the sample surface horizontally by a XY piezo stage and a topographical image of the sample is obtained. One of the key advantages of AFM is that it provides three dimensional images unlike SEM which provides two dimensional image of the sample.

The topographical images of thin films were taken by AFM (JEOL SPM 5200). SPM was used in non-contact mode with an area of $10 \times 10\ \mu m^2$ and $3 \times 3 \mu m^2$ for measuring roughness and grain sizes of thin films.

4.2.3 X-Ray Diffraction (XRD)

X-ray diffraction is an analytical technique commonly used for phase identification of a crystalline material, measuring crystallite size, and physical and mechanical properties of materials and thin films.

X-ray unit consists of an X-ray tube, a sample holder and an X-ray detector. In operational mode X-rays are generated in a cathode ray tube. The filament is heated to produce electrons and accelerating these electrons towards a target by applying a potential. The impact of electrons with target material, having sufficient energy, dislodges inner shell electrons producing characteristic X-rays spectra. The X-ray spectra consist of several components which include commonly K_α and K_β. These X-rays are then collimated and directed onto the specimen. When the incident X-rays impinging the sample satisfies the

Bragg equation, nλ=2dsinθ, constructive interference occurs. A detector records this diffracted signal, processes it, converts it to a count rate and output to an external monitor. The schematic diagram of XRD is shown in the Figure 4-4.

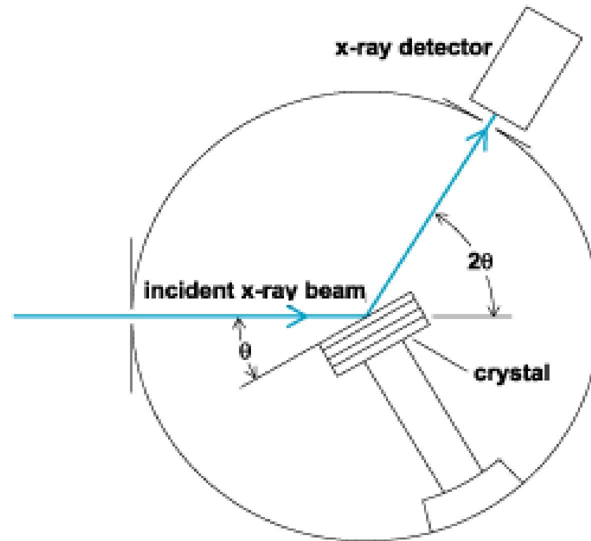

Figure 4-4: Schematic Diagram of XRD [4].

The crystalline analysis of thin films was conducted by X-ray diffractometer (STOE) using Cu kα radiation (λ=1.54052Å) target. XRD analysis was performed in 2θ range of 20-80 degrees. The step size was 0.04 and dwell time was 3 seconds. Mechanical and crystallographic properties were studied as a function of different deposition parameters using XRD.

4.2.4 Electrical Characterization

4.2.4.1 Four-Point Probe Method

4-point probe method is used to measure the resistivity of a material. Resistivity of a material is a property of the material in a given condition that measures the response of the material in terms of current flowing through it to an applied voltage. The electrical resistivity (δ) of a material is related to the resistance R and is given by given by:

$$R = \delta \frac{L}{A} \qquad \text{Equation 4-1}$$

where δ is the bulk resistivity in ohm-centimeters (Ω-cm), L is the length of the conductor in cm, and A is the cross-sectional area of the conductor in cm^2.

As shown in the figure 4.4 the four probes are touched with the flat sample, where the current I, enters through probe 1 and leaves it though probe 4. The voltage is measured

between the probes 2 and 3. All the probes are placed equidistant from one another at a distance d. The current density is given by

$$j = \frac{I}{2\pi R^2} \quad \text{Equation 4-2}$$

The voltage V_{23}, measure between probe 2 and 3, is related to the current flowing by

$$V_{23} = \int_{d}^{2d} \frac{I}{2\pi R^2} \rho dR = \frac{I\rho}{2\pi d}$$

Hence,

$$\rho = \frac{2\pi d}{I} V_{23} \quad \text{Equation 4-3}$$

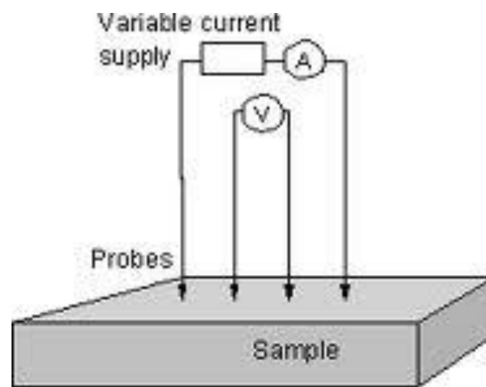

Figure 4-5: Diagram of Four Point Probe resistance measurement [5]

4.2.4.2 Hall Effect Measurement System

Electrical properties such as resistivity, carrier concentration and mobility were measured using Hall Effect Measurement System (Ecopia HMS-5000). The sheet resistance was determined by Four Point Probe method and then the resistivity was measured. Figure 4-6 shows the Hall Effect measurement system.

4.2.5 Scotch Tape Test

Scotch Tape test was performed to determine the adhesion of the film to the substrate. Adhesive tape of the same length was glued on the surface of the substrate and stripped with an approximately equal amount of force. After tape test surface morphology of thin films were examined using Optical Microscope (UMS-300).

Figure 4-6: Van der Pauw HMS-5000 Variable Temperature Hall Effect Measurement System by ECOPIA [6].

References

[1] http://www.alliance-concept.com/uk/dp650_uk.html (Alliance Concept DP650)
[2] P. E. J. Flewitt, and R. K. Wild, Physical Methods for Materials Characterization, Chapter 6 (IOP Publishing, Bristol) (1994)
[3] http://www.edinformatics.com/nanotechnology/atomic_force_microscope.htm (Nanotechnology & the Atomic Force Microscope)
[4] http://ehs.columbia.edu/News%20Letter/FA09Page4.html (X-Ray Diffraction System)
[5] http://www.chm.bris.ac.uk/pt/diamond/jamespthesis/chapter2.htm (Film Analysis)
[6] http://www.four-point-probes.com/hms5000.html (Four Point probe Bride Technology)

CHAPTER NO 5

Results & Discussion

Characterization of Molybdenum Sputtered Thin Films

5.1 STUDY OF MOLYBDENUM SPUTTERED THIN FILMS

In this study, molybdenum (Mo) thin films were deposited using DC-plasma magnetron sputtering. Deposition parameters such as Ar pressure, deposition power and substrate temperature were analyzed using characterization tools in order to find optimum deposition conditions to obtain thin films of back contact material with high electrical conductivity for $Cu(In,Ga)Se_2$ based thin films solar cells.

5.2 ARGON PRESSURE

Mo thin films were prepared on soda lime glass substrates using DC-plasma magnetron sputtering. Thin films prepared as a function of Ar pressure are to be discussed in this section. The results obtained from different characterization tools and related discussions on each of these results are as under;

The results of XRD measurements are shown in Table 5-1. The X-ray diffraction spectra of Mo thin films grown at different working pressures are shown in the Figure 5-1. From the figure it is clear that single main peak was observed with orientation along (110) direction showing the preferred orientation of Mo thin films. As the Ar flow rate or Ar pressure was increased, the intensity of diffracted plane (110) plane was decreased, which were probably either due to decrease in growth energy or increase in Ar impurities. This trend also indicated that Mo films sputtered at lower pressure shows higher crystallinity than films sputtered at higher pressure. This can be correlated as at lower working pressure the dense microstructure has been obtained.

The average particle size or crystallite size can be calculate from the broadening of the (110) peak using Scherer's equation [1].

$$L = \frac{K\lambda}{B\cos\theta} \qquad \text{Equation 5-1}$$

Where K (K=0.94) is the Scherer's constant, L is the crystallite size, λ (CuK_{α}= 1.5404Å) is the wavelength of the X-ray and B is the FWHM of diffraction peak at θ.

The crystallite size was found to increase as the argon pressure increases, as shown in Figure 5-2. As the Ar pressure increases the intensity of diffracted plane (110) decreases which were probably due to increase in Ar impurities or decrease in growth energy.

The shifting of peaks from actual positions indicates the internal residual stresses in the films. The residual stress calculations were made from XRD data by strain equation. Using Bragg's formula the inter-planar spacing d_{110} was calculated. The % strain in the films is then calculated by the following equation.

$$\text{Strain}\ (\%) = \frac{\Delta a}{a} \times 100\% \qquad \text{Equation 5-2}$$

Where “a” is the lattice constant (for Mo, a=0.31472nm). It is the main parameter to determine whether the strain is compressive or tensile [2]. The origin of the strain profiles in Mo thin films usually related to several factors including voids, crystallographic flaws, oxygen content and Ar impurities [3]. The high strain in the films can cause adhesion problems and long term reliability. Most of the Mo thin films fabricated in this work were under tensile strain. Figure 5-3 shows that as the Ar pressure increases the % strain in the films deceases. The maximum strain obtained was 2.320% for Ar pressure of 0.0123mbar.

The effect of peak broadening is due to both small crystallite size and strain. For calculating %age contribution to peak broadening, it is required to have multiple XRD data for single experiment. Since we have only a single value of XRD peak for single experiment, it is difficult to calculate the %age contribution of peak broadening.

Table 5- 1: XRD, electrical and adhesion measurements as a function of Ar pressure, deposition power and substrate temperature for DC-sputtered Mo thin films.

Deposition Conditions			Thickness (nm)	Rate (nm/s)	Crystallite Size (nm)	Strain (%)	Resistivity (Ω.cm)	Tape Test
Pressure (mbar)	Power (W)	Temp (^{0}C)						
0.0123	100	RT	562	0.67	15.6	0.684	4.85×10^{-04}	Pass
0.0123	100	400	872	1.04	4.6	2.320	3.08×10^{-04}	Pass
0.0123	200	RT	545	1.13	21.1	0.564	2.57×10^{-04}	Pass
0.0123	200	400	327	0.73	14.5	0.728	1.72×10^{-04}	Pass
0.002	100	RT	645	0.72	7.9	1.397	3.93×10^{-04}	Fail
0.002	100	400	618	0.69	-----	1.02	3.07×10^{-04}	Fail
0.002	200	RT	543	1.13	13.5	0.840	7.15×10^{-05}	Fail
0.002	200	400	574	1.29	-----	1.03	7.02×10^{-05}	Fail

.

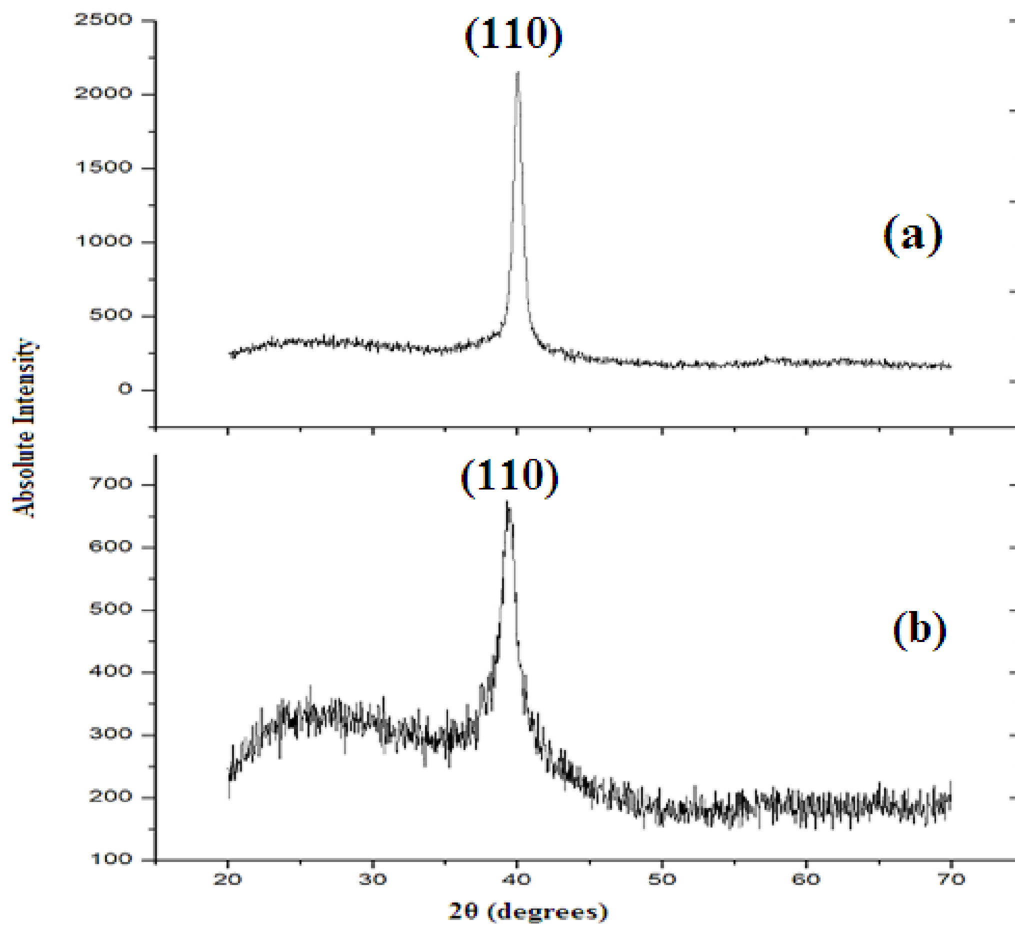

Figure 5-1: Typical XRD patterns of Mo films under various Ar pressures with an orientation along (110) direction.

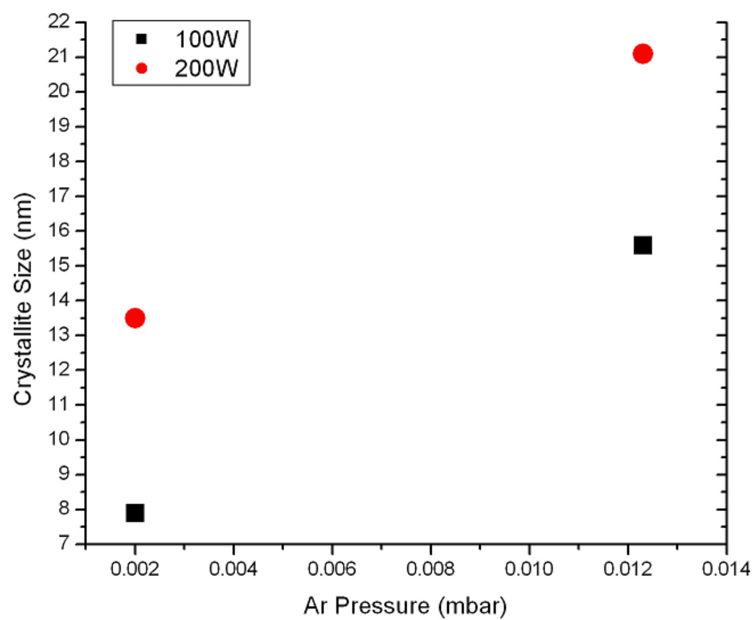

Figure 5-2: Crystallite size of Mo thin films as a function of Ar pressure.

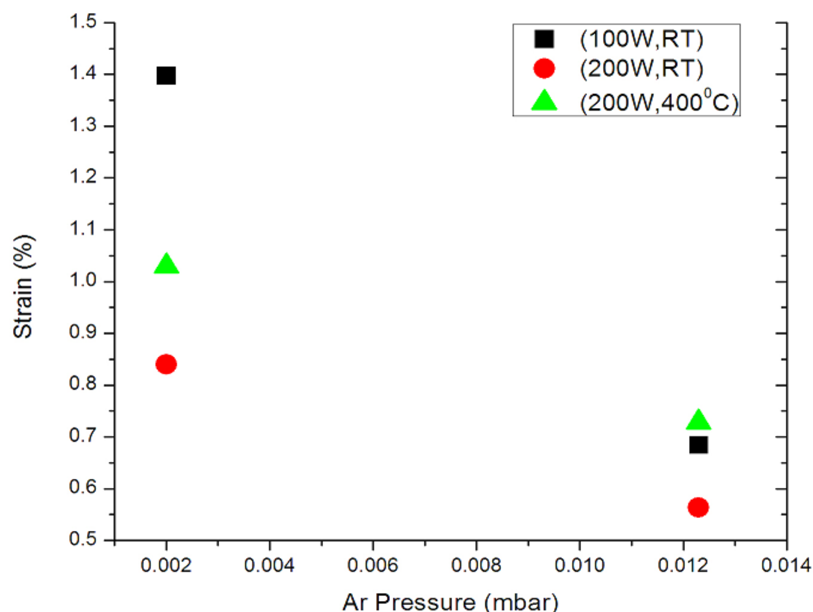

Figure 5-3: %Strain in Mo thin films as function of Ar pressure.

Scanning Electron (SEM) micrographs of Figure 5-4 shows the surface morphologies of the sputtered Mo thin films at different working gas pressures. Literature review revealed that films sputtered at higher pressures, typically in the range of 0.011-0.027mbar, exhibited porous microstructures while films sputtered at lower chamber pressures (0.0002-0.0094mbar) exhibited dense microstructures [4]. This is primarily due to the fact that, upon increasing chamber pressure, the sputtered species undergo more inelastic scattering incidents which, in turn, introduce shadowing effect resulting in porous film structure. In our case, cross-sections of films deposited under all experimental conditions exhibited minimum or no porosity, as shown in Figure 5-5. In other words, the value of chamber pressure (0.002mbar or 0.0123mbar) did not appear to incorporate significant levels of porosity into films. Figure 5-4 shows a smooth morphology and revealing dense microstructure. From higher magnification images of the film cross-sections, the average thickness values were estimated and subsequently, film growth rate for each experimental condition was calculated, as listed in Table 5-1. Figure 5-4(a) shows that the surface of the film is bulging out at different places, this is due to the fact that stresses were observed in Mo thin films. At high magnification (figure 5-4(c)) the films again shows a very smooth morphology and as the chamber increases the surface of the films becomes more rough as shown in the figure 5-4(d). The cross-sectional view of the Mo films deposited is shown in the figure 5-5. The cross-sectional view indicated a granular (figure 5-5 (a)), diffuse (figure 5-5 (b,d,e,f)) and columnar

morphology (figure 5-5(c)). It was observed from the cross-sectional morphology that different thickness of films deposited on the substrate as shown in the table 5-1. This was not in agreement with the experimental data table (Table 4-1) which shows that 1μm thickness was kept constant for all the deposition parameters.

The electrical resistivities of Mo thin films were determined from Hall Effect measurement system using Four Point Probe method. The values of electrical resistivities as function of Argon pressure are reported in Table 5-1. Figure 5-6 shows the variation of electrical resistivity of the sputtered Mo thin films with respect to the Ar pressure. It was observed that electrical resistivity decreases with decreasing Ar pressure. The film prepared at Ar Pressure of 0.002mbar, a substrate temperature of 400 ^{0}C and deposition power of 200W was found to have a resistivity equal to 7.02×10^{-05} Ω-cm, corresponding to the lowest resistivity value for the Mo thin films prepared in this research work. The electrical resistivity values obtained falls in the range of the values (0.1×10^{-04} - 2.5×10^{-04}Ω-cm) reported by Scofield et al. [5] for Mo films deposited on soda-lime glass substrates using a DC-magnetron sputtering system.

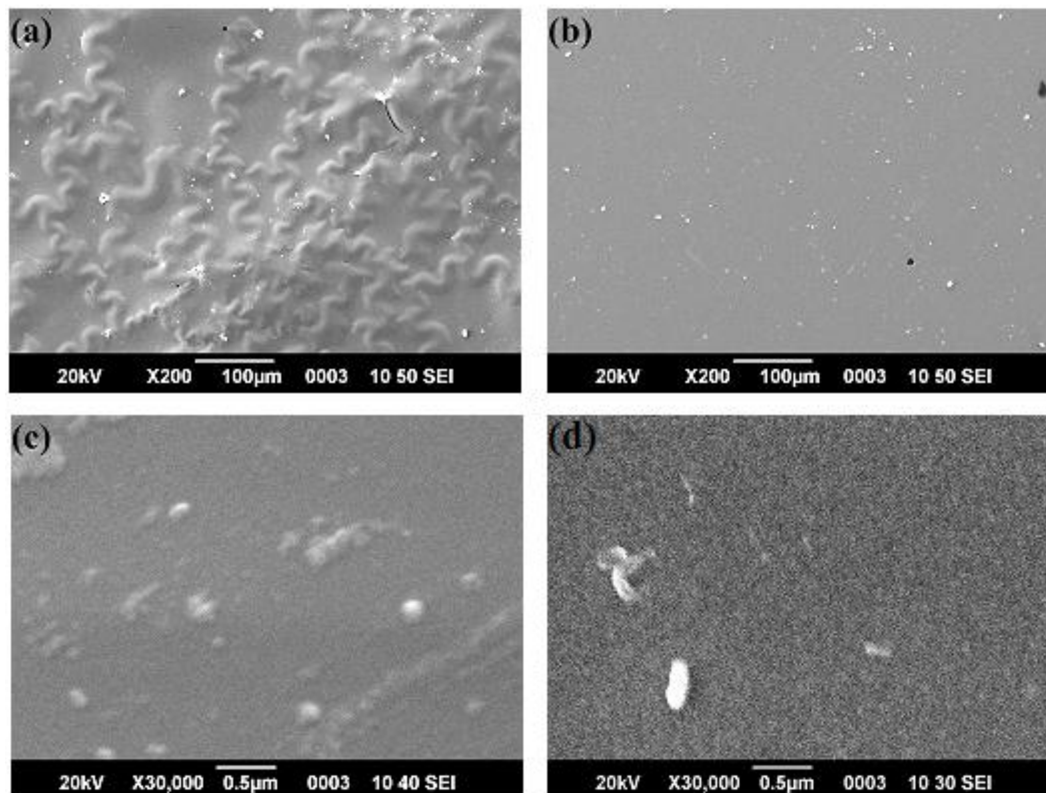

Figure 5-4: SEM morphologies of Mo films (a) 0.002mbar, 200W, RT (b) 0.0123mbar, 200W, RT (c) and (d) magnified images of the two samples respectively.

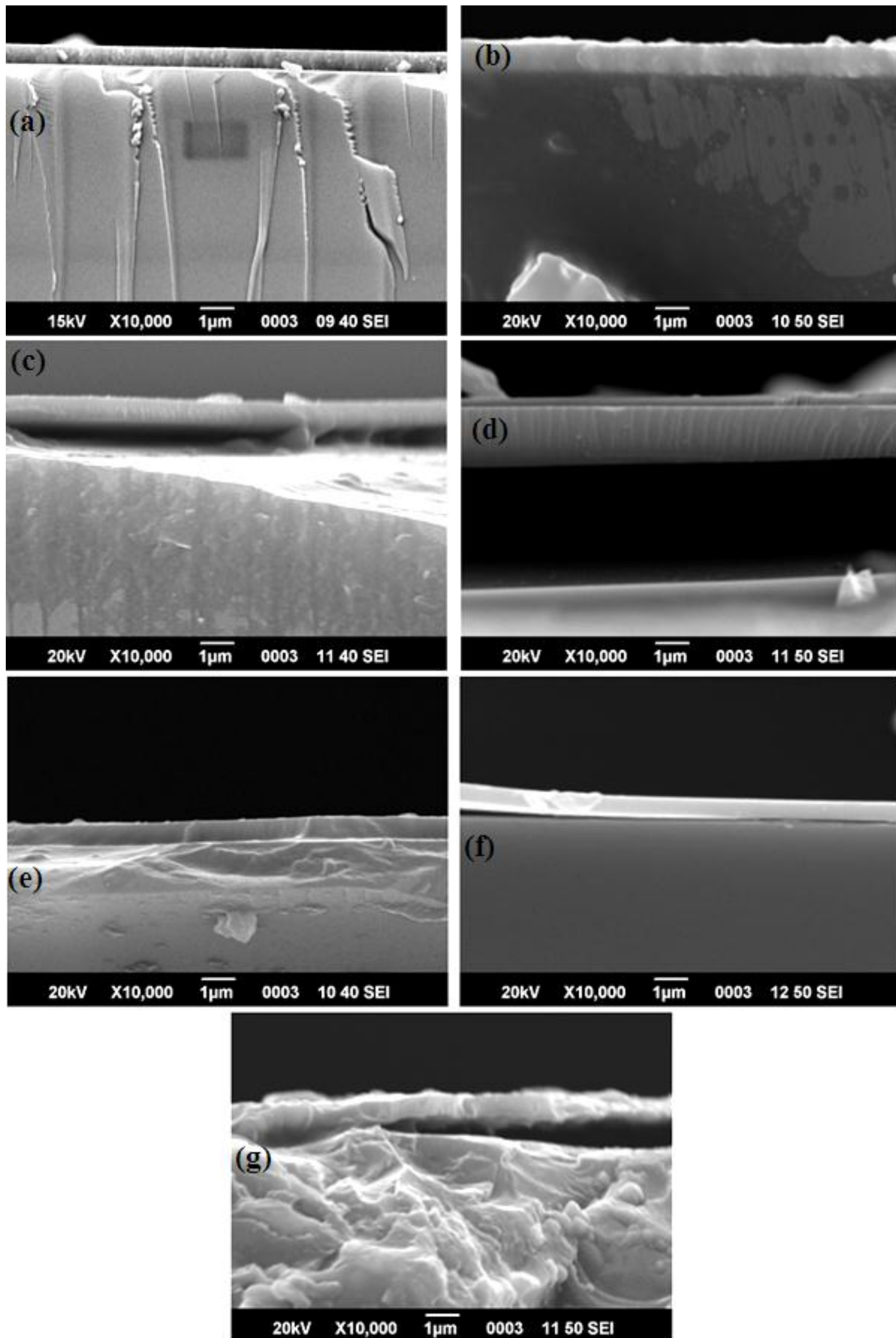

Figure 5-5: SEM cross-sections of Mo thin films (a) 0.0123mbar ,100W, RT (b) 0.0123mbar, 100W, 400^0C (c) 0.0123mbar , 200W, RT (d) 0.0123mbar, 200W, 400^0C (e) 0.002mbar, 100W, 400^0C (f) 002mbar, 200W, RT (g) 002mbar, 200W, 400^0C.

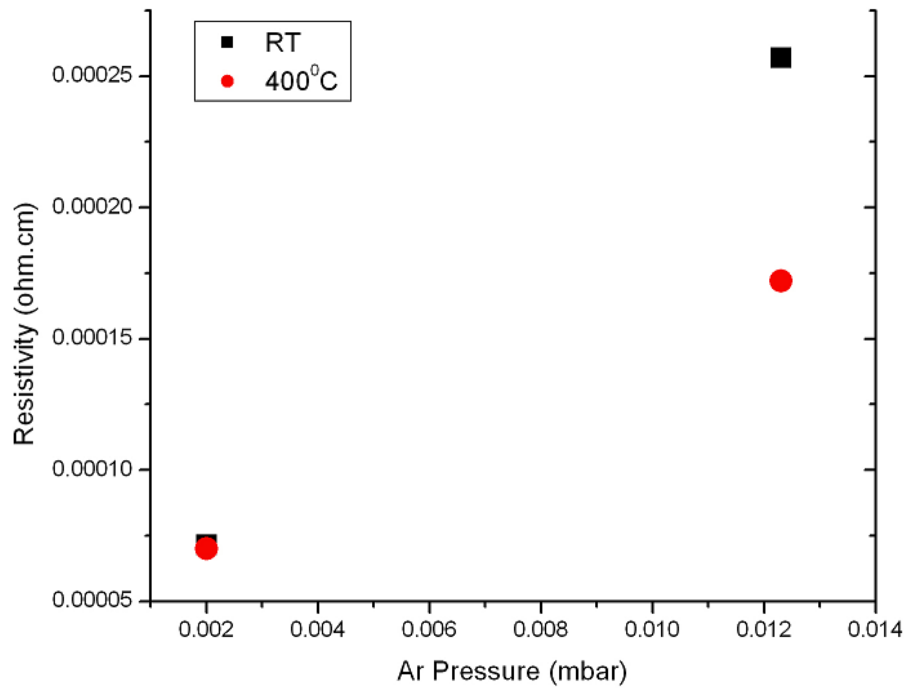

Figure 5-6: Resistivity of Mo films as a function of Ar pressure.

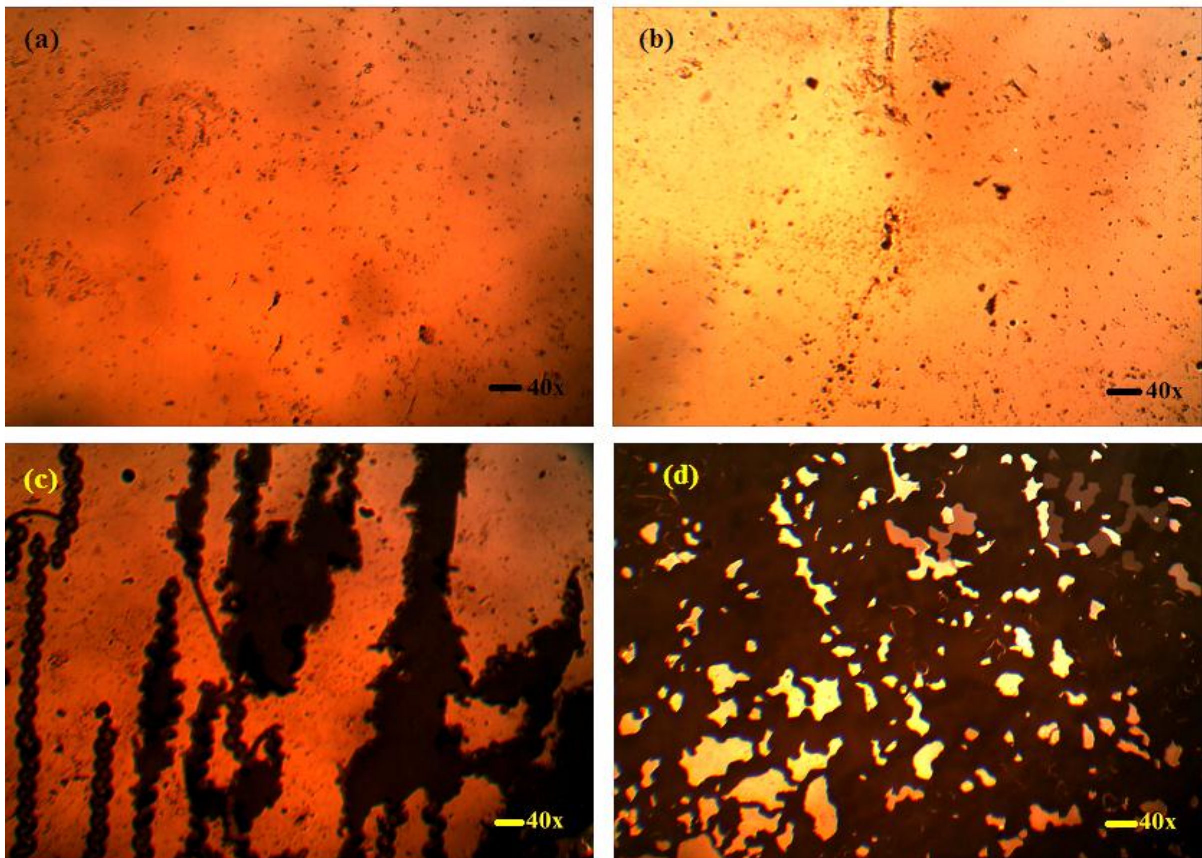

Figure 5-7: Optical images of Mo thin films after the scotch tape test at various deposition parameters (a) 0.0123mbar, 200W, 400^0C (b) 0.00123mbar, 100W, 400^0C (c) 0.002mbar, 100W, RT (d) 0.002mbar, 100W, 400^0C.

The adhesion of the films to the substrate was performed using scotch tape test. The tape was glued on the surface of thin films and stripped manually by applying force with hand. It was observed that films prepared at higher working gas pressure passed the tape test while the films prepared at lower working gas pressure fail the tape test. Figure 5-7 shows the optical microscope images of Mo thin films. The figure 5-7 (a,b) shows that at high Ar pressure the Mo films exhibit good adhesion to the substrate. But decreasing Ar pressure worsens the adhesion property. This is due to the fact that as Ar pressure decreases the % strain in the films increases. Mo layer appears to have flaked partly along the edges of the cuts and wholly on different parts of the square as shown in the figure 5-7 (c,d).

5.3 DEPOSITION POWER

In this section Mo thin films deposited at different deposition powers are to be discussed. The X-ray diffraction patterns grown from deposition powers (100W-200W) are shown in Figure 5-7. It can be seen that the crystallites of Mo films maintain the cubic crystal structure (JCPDS Card No. 3-065-7442). From figure 5-8 it is clear that Single main peak was observed with an orientation along (110) direction. The crystallite size was found to increases as the deposition power increases (figure 5-9). Figure 5-8 shows that the intensity of the (110) peak increases significantly as the deposition power increases. It was observed that the films deposited at high deposition power the kinetic energy of the species increases resulting in 3D Volmer-Weber growth. The films prepare at high deposition power were found to have high dense microstructure resulting the crystallized with large grains, whereas the films deposited at low deposition power are essentially more random and disoriented in nature [6].

The shift of the (110) peak along 2θ allowed us to calculate strain in thin films. All the films showed tensile strain. It has been suggested that voids, crystallographic flaws, oxygen or argon impurities could be responsible for the stress in the sputtered Mo films [3]. It is argued that these effects are related to the frequency of gas phase collisions in the sputtering system which alters the kinetic energy of both Argon and Mo atoms.

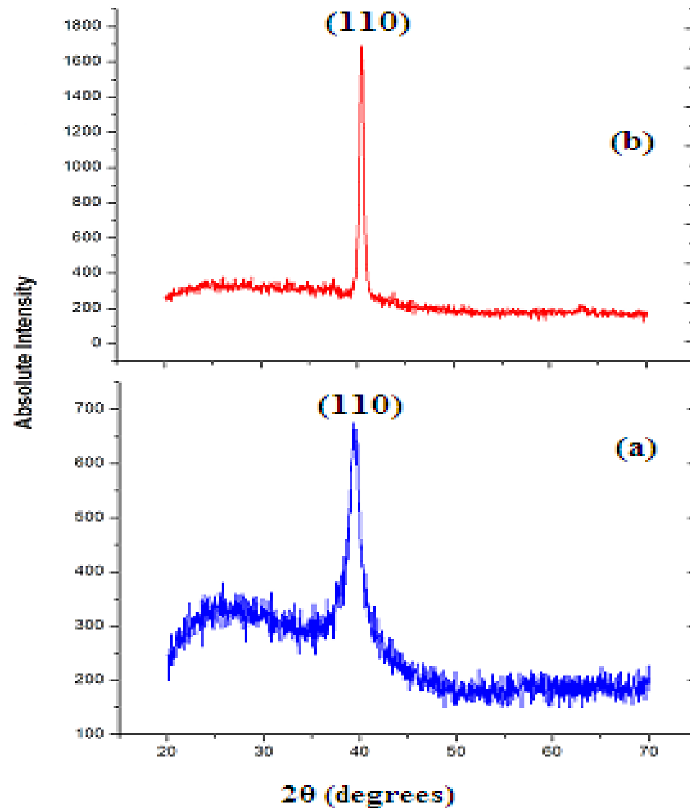

Figure 5-8: Typical XRD patterns of Mo films at (a) 100W (b) 200W

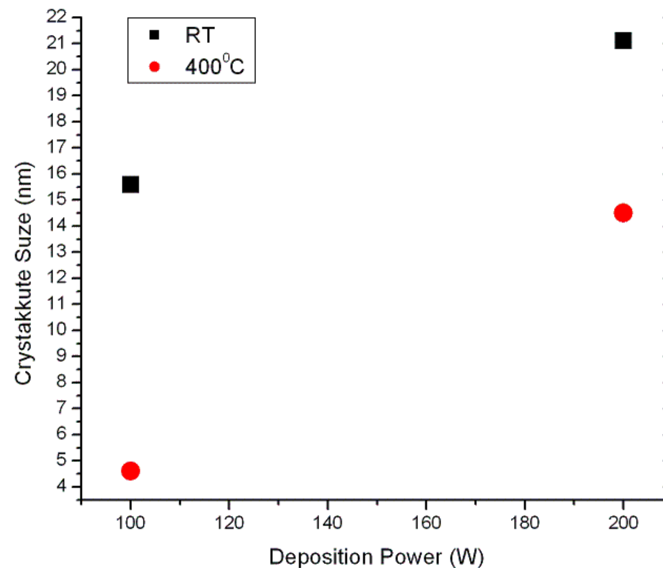

Figure 5-9: Crystallite size of Mo thin films as a function of deposition power.

Scanning Electron (SEM) micrographs of Figure 5-10 shows the surface morphologies of the sputtered Mo thin films at different deposition powers. Literature review reveal that films sputtered at lower deposition power exhibited porous microstructures while films sputtered at higher deposition power exhibited dense microstructures [4]. At higher deposition power, deposition rate increases so that number of species arriving at the substrate

increases resulting in a denser microstructure while at low deposition power, deposition rate decreases and the number of species arriving at the surface of the substrate becomes less resulting in a porous microstructure. However, in our case no porous microstructure was observed. Figure 5-10 (a,b) shows a smooth morphology and revealing dense microstructure. Figure 5-10(a) shows that the surface of the film is rough and less dense. As the deposition power increases the surface becomes more smooth and compact as shown in the figure 5-10(b).The cross-sectional view of the Mo films deposited shows granular morphology as shown figure 5-10(d). The EDS analysis confirms that 100% Mo thin films was deposited.

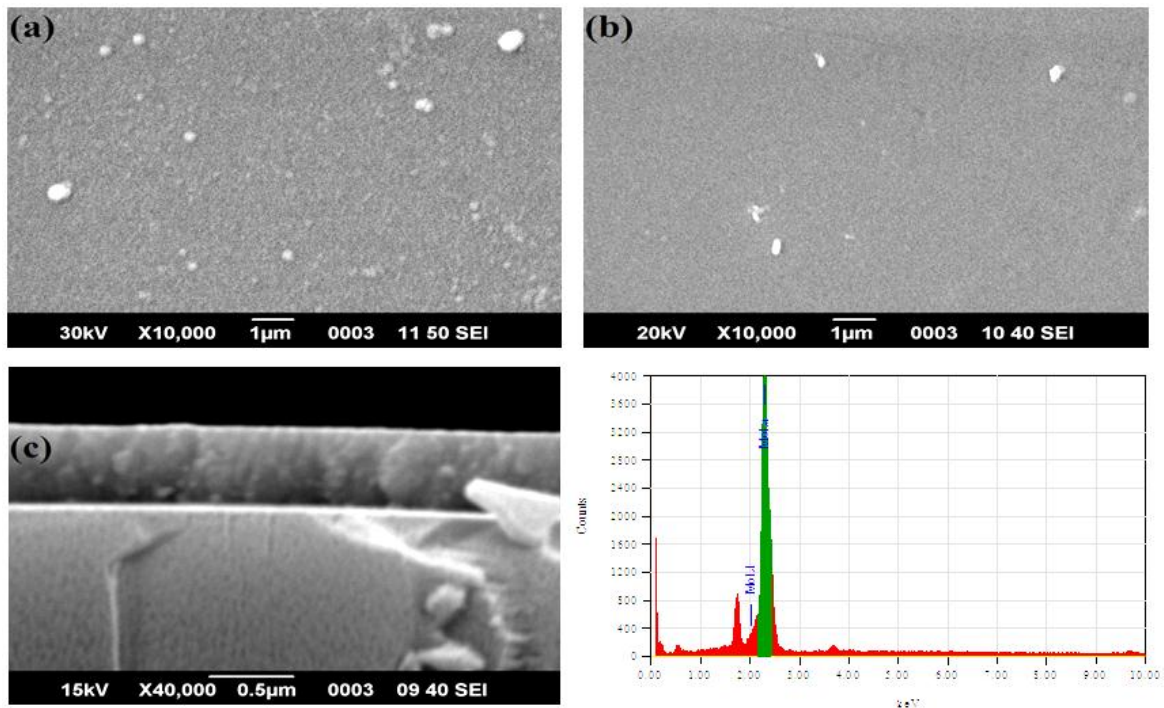

Figure 5-10: SEM micrographs of Mo thin films (a) 100W, RT, 0.0123mbar (b) 200W, RT, 0.0123mbar (c) SEM Cross-section (d) EDS analysis

Figure 5-11 shows AFM images of Mo thin films sputtered at deposition power of 100W and 200W. To study the surface features of Mo films, it is necessary to measure the main surface roughness parameters of these films, namely RMS and Ra. Generally, the surface roughness at a certain area is determined by the height differences of all the distinct points at this area. RMS roughness is the mean of the root for the deviation from the standard surface to the indicated surface. Ra represents the three-dimensional expansion of the center line mean roughness so that it is applicable to the measurement surface. The surface roughness of the films increased as the deposition power was increased [7]. The average surface roughness R_a for the film deposited at 100W and 200W was about 0.962nm and 1.34nm respectively. The root means square roughness R_q (RMS) also increases as the

deposition power increases as shown in the Figure 5-12. This result is attributed to large increase of the number of sputtered Mo molecules arriving at the surface of the substrate.

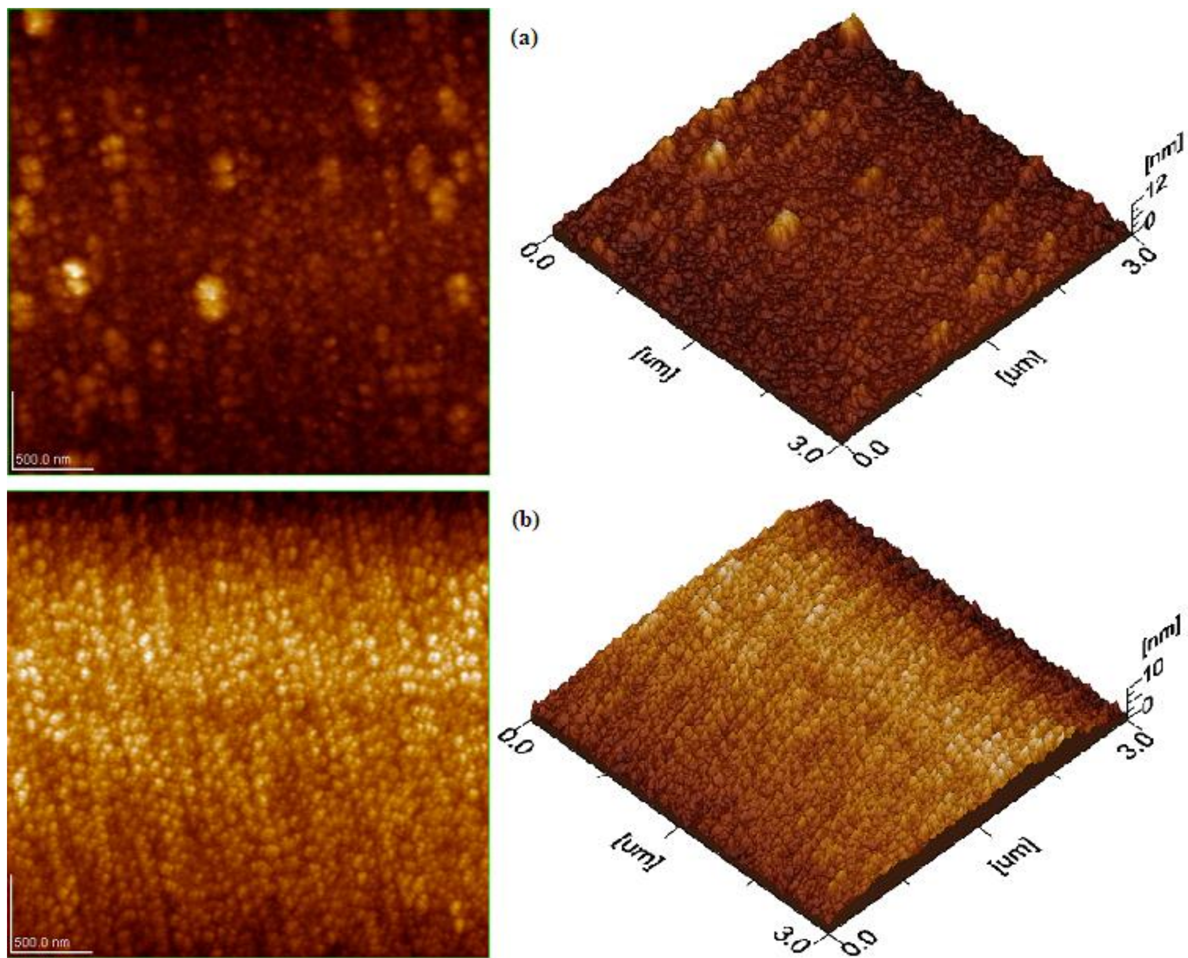

Figure 5-11: AFM morphologies of Mo thin films for deposition powers of (a) 100W (b) 200W.

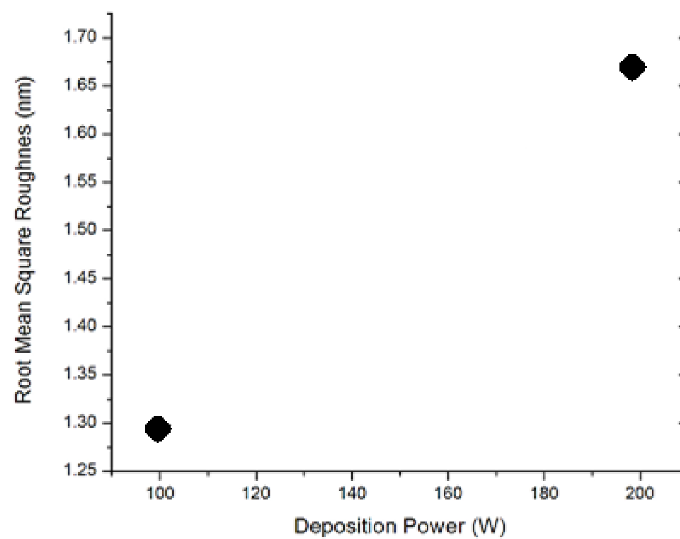

Figure 5-12: Root Mean Square roughness of Mo films as function of deposition power.

The resistivity of Mo films was measured using Vander Paw method. In confirmation with the Gardillo et al. [8] results, the resistivity decreases by increasing the deposition power as shown in Figure 5-13. Deposition power is plotted against the resistivity values for the deposition parameters of Ar pressure and substrate temperature. This decrease in resistivity is attributed to the dense microstructure at high deposition power which enhances the rapid growth of relatively thick film.

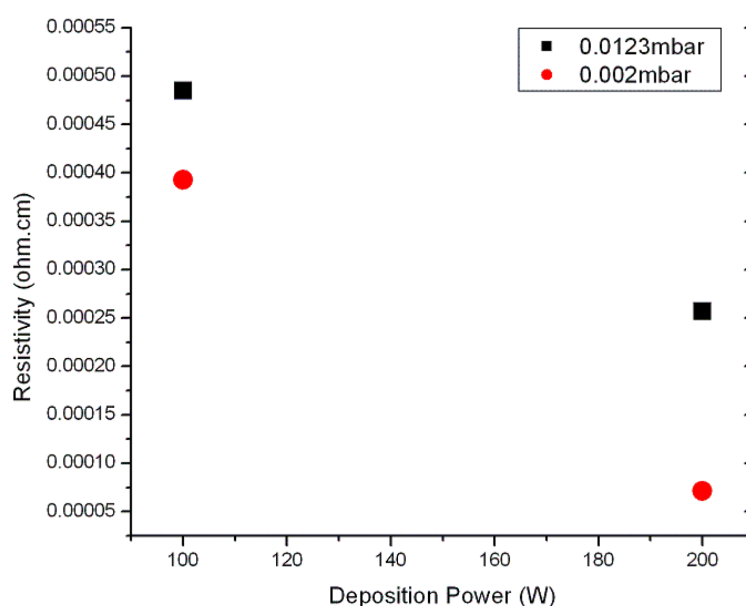

Figure 5-13: Resistivity of Mo films as a function of deposition power.

The adhesion of the film was investigated with scotch tape adhesion test by gluing the tape on the surface of the film and stripping it manually by applying force manually. The adhesion property worsens as the deposition power increases (Figure 5-11).The delamination of the film from the substrate at high deposition power can be attributed to a fast deposition rate of Mo on the substrate. Consequently, the successive deposited Mo layers lack the appropriate time to strongly adhere to the substrate.

5.4 SUBSTRATE TEMEPERATURE

In this section Mo thin films deposited at different substrate temperatures are to be discussed. The X-ray diffraction patterns grown from substrate temperatures (RT-400^{0}C) are shown in Figure 5-14. It can be seen that the crystallites of Mo films maintain the cubic crystal structure (JCPDS Card No. 3-065-7442). Single main peak was observed with an

orientation along [110] direction. The Figure 5-14 shows that the intensity of the (110) peak increases significantly as the substrate temperature increases. The crystallite size was calculated from the Scherer's equation [1]. It was observed that crystallite size decreases from 21.1nm to 14.5nm as the substrate temperature increases from room to 400^0C as listed in the data Table 5-1. Substrate temperature dependence of crystallinity may be interpreted as. When substrate temperature increases, the films become non-stoichiometric [9]. The oxygen deficiency leads to the growth of less homogeneous films with more crystallographic faults, and a decrease in the long-range order in the deposited films. Hence as the temperature becomes higher and higher the crystallinity of the deposited films becomes poorer.

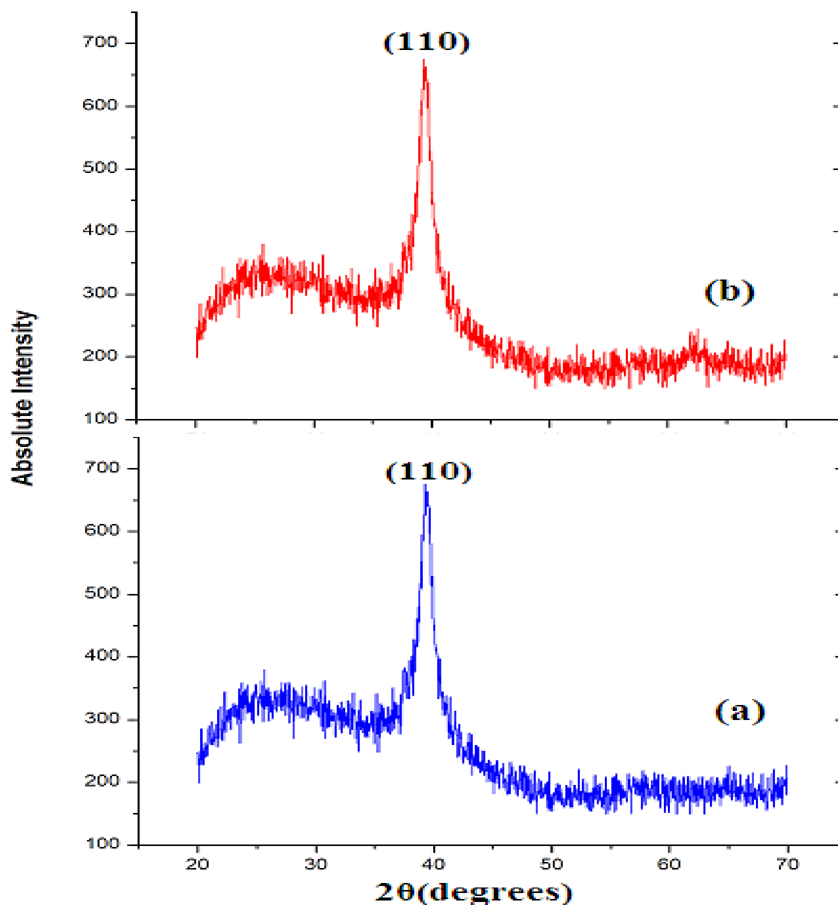

Figure 5-14: Typical XRD patterns of Mo films at substrate temperature (a) RT (b) 400^0C with an orientation along (110) direction.

Figure 5-15 shows AFM images of Mo thin films prepared at substrate temperature of 23^0C and 400^0C. The surface roughness of the films increased as the substrate temperature was increased. The average surface roughness R_a for the film deposited at 23^0C and 400^0C was about 1.16nm and 1.74nm respectively. The root means square roughness R_q (rms) also increases as the substrate temperature increases as shown in the Figure 5-16. Increasing the

substrate temperature increases the film quality because thermal energy enhances the surface mobility of the arriving species. As the substrate temperature increases, grain size increases and the surface becomes rougher and relatively less dense.

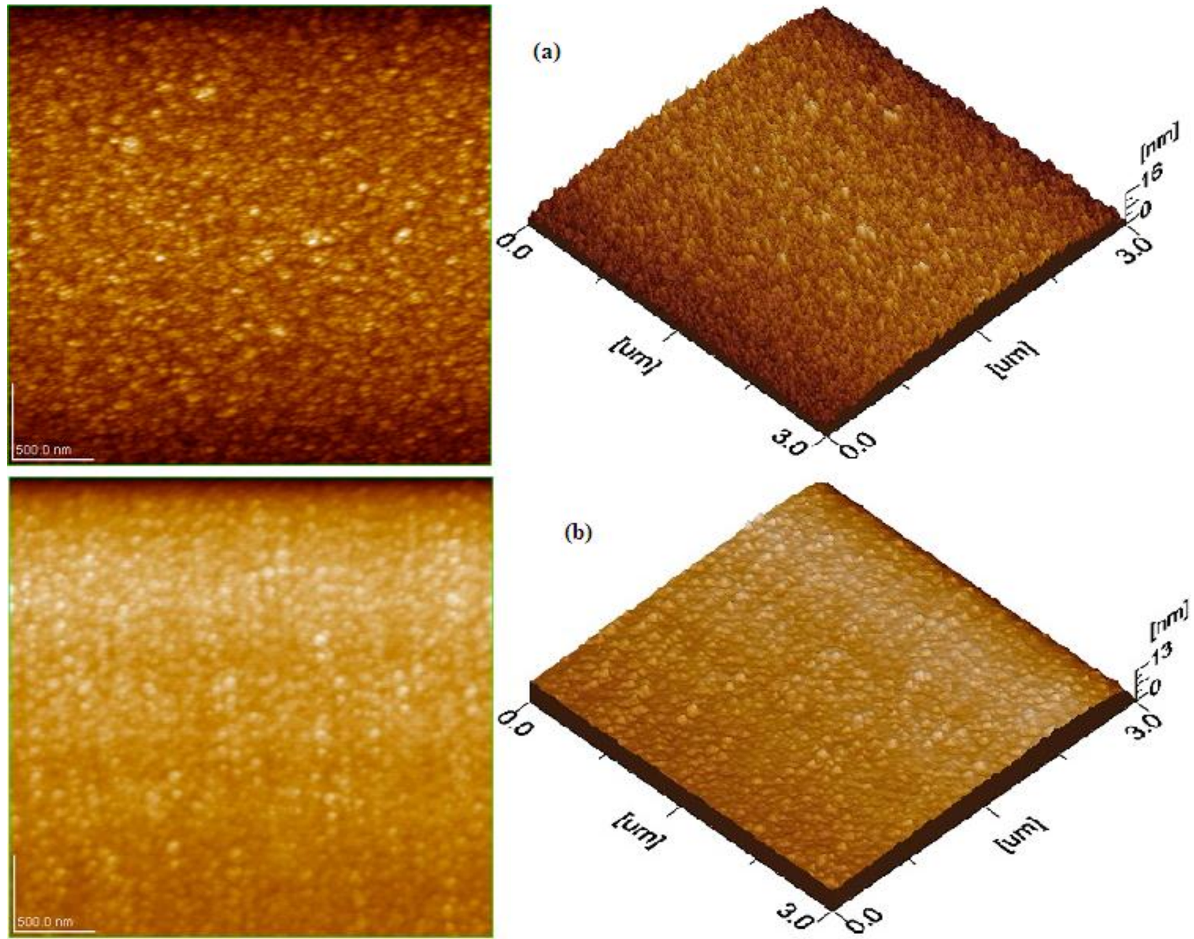

Figure 5-15: AFM morphologies of Mo thin films for substrate temperatures of (a) RT (b) 400^0C

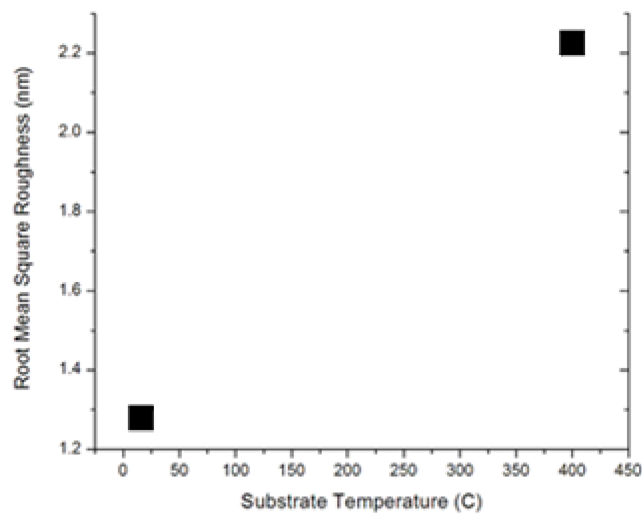

Figure 5-16: Root Mean Square roughness of Mo films as function of substrate temperature.

The resistivity of Mo films was measured using Vander Paw method. In confirmation with the Gardillo et al. [8] results, the resistivity decreases by increasing the substrate temperature as shown in Figure 5-17. Substrate temperature is plotted against the resistivity values for the deposition parameters of Ar pressure and deposition power. This decrease in resistivity is attributed to the dense microstructure at high substrate temperature which enhances the formation of clusters in the film by making reduction in the grain boundaries potential barrier height as well as in the number of grain boundaries and enhancing the carrier mobility of the charges [8]. This explains the result that lowest resistivity was observed at deposition power of 400^0C.

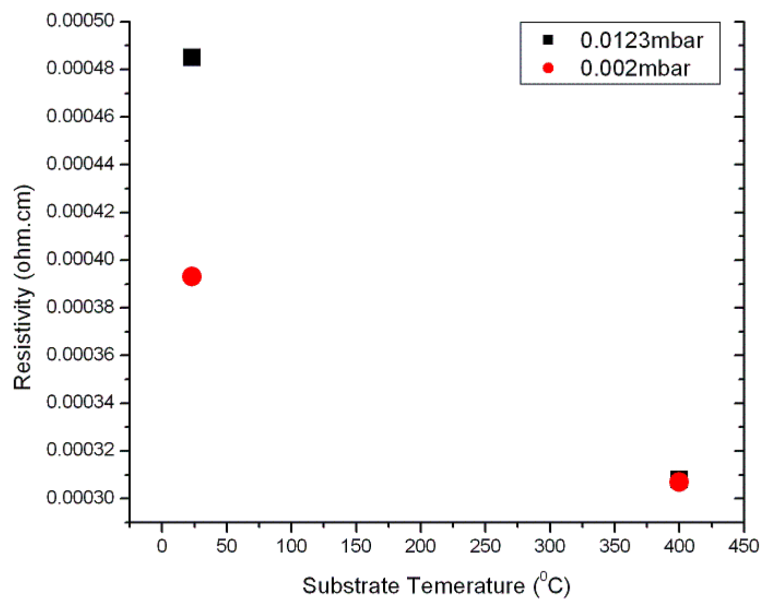

Figure 5-17: Resistivity of Mo thin films as a function of substrate temperature.

References

[1] N. Kasai, M. Kakudo, X-ray Diffraction by Macromolecule (New York: Springer) pp. 364–5 (2005)
[2] JCPDS card 42-1120 Mo cubic a = 0.31472 nm.
[3] S. G. Malhotra, Z. U. Rek, S. M. Yalisove, S. M., J. C. Bilello, "Strain gradients and normal stresses in textured Mo thin films." J. Vac. Sci. Technol. A 15, 345 (1997).
[4] T. J. Vink, M. A. J. Somers, J. L. C. Daams and A. G.Driks, J. Appl. Phys. 70, 4301 (1991)
[5] J.H. Scofield, A. Duda, D. Albin, B.L. Ballard, P.K. Predecki, Sputtered molybdenum bilayer back contact for copper indium diselenide-based polycrystalline thin-film solar cells, Thin Solid Films 260 pp 26–31 (1995)
[6] S. Y. Kuo, L. B. Chang, M. J. Jeng, W. T. Lin, Y. T. Lu, S. C. Hu, Effects of Growth Parameters on Surface-morphological, Structural and Electrical Properties of Mo Films by RF Magnetron Sputtering, Mater. Res. Soc. Symp. Proc. Vol. 1123 (2009)
[7] K. H. Yoon, S. K. Kim, R. B. V. Chalapathy, J. H. Yun, J. C. Lee, J. Song, Characterization of a Molybdenum Electrode Deposited by Sputtering and its Effect on Cu(In,Ga)Se2 Solar Cells, Journal of the Korean Physical Society, Vol. 45, pp. 1114-1118 (2004)
[8] G. Gordillo, F. Mesa, C. Caldero´ n, Electrical and morphological properties of low resistivity Mo thin films prepared by magnetron sputtering, Brazilian Journal of Physics V36 (3B), pp.982–985 (2006)
[9] S.S. Lin, J.L. Huang and D.F. Lii: Surf. Coat. Technol., 176, 173 (2004)

CHAPTER NO 6

CONCLUSIONS

6.1 CONCLUSIONS

Thin films of Molybdenum were prepared on soda lime glass substrates using DC-magnetron sputtering system. The effects of deposition parameters, namely Ar pressure, deposition power and substrate temperature on film microstructure, resistivity and interfacial strength of the Mo thin films have been investigated. The following conclusions were drawn from this experimental work.

- For the range of synthesis conditions investigated, deposited films were found to exhibit single diffraction peak corresponding to (100) plane. This finding is in agreement with reported literature. Film morphology was found to be very smooth with a low average surface roughness value. The degree of film density varied depending on processing conditions and was examined to deteriorate upon increasing pressure or decreasing substrate temperature.
- Minimum value of electrical resistivity, as measured using Hall effect apparatus, was $\sim 0.7\times10^{-06}$ Ω.cm for films produced at 200W, 0.002mbar and 400^{0}C. This combination of processing parameters suggests growth of dense films due to high energy of species incident onto the substrate as well as greater degree of surface and volumetric diffusion during film growth (owing to high substrate temperature). Compared with literature, this value falls in the range (0.1 – 1.1 μ Ω.cm) reported.
- Thin films investigated showed characteristics internal residual stresses produced as function of chamber pressure. Within the range of deposition parameters studied, Mo thin films were under tensile stresses.
- Higher values of chamber pressure, power and/or low substrate temperatures introduce micro-voids into the film which lead to failure of the film. In other words, the likelihood of an interfacial failure (i.e. delamination) decreases.

6.2 FUTURE RECOMMENDATIONS

For more productive results and applications point-of-view, further work should be carried out to address the following issues.

- This study produced films with internal tensile stresses. Synthesis conditions can be explored to obtain films with compressive stresses, so that Mo bilayer configuration can be obtained, suitable for thin film solar cells.
- Other methods such as colloidal deposition route can also be explored to obtain Mo films with similar or even better performance attributes of back contact material in CIGS solar cells.
- Corrosion of molybdenum is one of the few known issues and has been reported to contribute to module degradation in accelerated lifetime testing of CIGS based thin film solar cells. It is possible that the stability of Mo could be improved by using Mo-based alloys instead of pure Mo.
- One of the disadvantages of molybdenum is its poor optical reflection. To improve its optical reflectance it is required to reduce the thickness of the absorber layer in CIGS based solar cells.